UNCI
SECURITY

AD-A256 342

(2)

REPORT DOCUMENTATION PAGE

Form Approved
OMB No. 0704-0188

DTIC ELECTE OCT 14 1992 S B D

1a. REPORT SECURITY CLASSIFICATION Unclassified	1b. RESTRICTIVE MARKINGS
2a. SECURITY CLASSIFICATION AUTHORITY	3. DISTRIBUTION / AVAILABILITY OF REPORT Approved for public release; distribution is unlimited.
2b. DECLASSIFICATION / DOWNGRADING SCHEDULE	
4. PERFORMING ORGANIZATION REPORT NUMBER(S)	5. MONITORING ORGANIZATION REPORT NUMBER(S) AFOSR-TR- 92 0908
6a. NAME OF PERFORMING ORGANIZATION Northwestern University	6b. OFFICE SYMBOL (If applicable)
6c. ADDRESS (City, State, and ZIP Code) Evanston, IL 60201	7a. NAME OF MONITORING ORGANIZATION AFOSR/NC
	7b. ADDRESS (City, State, and ZIP Code) Building 410, Bolling AFB DC 20332-6448
8a. NAME OF FUNDING / SPONSORING ORGANIZATION AFOSR	8b. OFFICE SYMBOL (If applicable) NC
8c. ADDRESS (City, State, and ZIP Code) Building 410, Bolling AFB DC 20332-6448	9. PROCUREMENT INSTRUMENT IDENTIFICATION NUMBER AFOSR-88-0297
	10. SOURCE OF FUNDING NUMBERS

PROGRAM ELEMENT NO.	PROJECT NO.	TASK NO.	WORK UNIT ACCESSION NO.
61102F	2303	A2	

11. TITLE (Include Security Classification)
(U) EXPERIMENTAL AND THEORETICAL INVESTIGATION OF SURFACE CHEMISTRY INDUCED BY DIRECT AND INDIRECT ELECTRONIC EXCITATION

12. PERSONAL AUTHOR(S)
S.J. Garrett

13a. TYPE OF REPORT	13b. TIME COVERED	14. DATE OF REPORT (Year, Month, Day)	15. PAGE COUNT
Final	FROM 8/88 TO 1/92	92/8/1	63

16. SUPPLEMENTARY NOTATION

17. COSATI CODES			18. SUBJECT TERMS (Continue on reverse if necessary and identify by block number)
FIELD	GROUP	SUB-GROUP	

19. ABSTRACT (Continue on reverse if necessary and identify by block number)

A combined theoretical and experimental investigation of the photochemistry of methyl iodide on rutile at 100-110 K has been attempted in order to assess the importance of each of the possible direct or indirect photon absorption processes. We have used x-ray photoelectron spectroscopy (XPS), temperature programmed desorption (TPD) and a UHV chamber designed for 257-351 nm laser irradiation of the adlayer followed by time-of-flight mass spectrometry (TOF-MS). We have observed that following irradiation, methyl photofragments are ejected into the vacuum. These photofragments possess a characteristic translational energy distribution extending up to 1.9 eV in the case of 257 nm radiation, which varies somewhat with photodissociation wavelength and methyl iodide coverage. Two broad peaks are visible in the translational energy distribution corresponding to methyl fragments with energies of 1.1 and 0.03 eV. The higher energy fragments are produced with a relatively narrow angular distribution and some vibrational excitation in the v"=1 and v"=2 "umbrella" modes of the methyl radical, whilst those of low translational energy /cont

20. DISTRIBUTION / AVAILABILITY OF ABSTRACT	21. ABSTRACT SECURITY CLASSIFICATION
☐ UNCLASSIFIED/UNLIMITED ☐ SAME AS RPT ☐ DTIC USERS	UNCLASSIFIED
22a NAME OF RESPONSIBLE INDIVIDUAL L W BURGGRAF, LT COL, USAF	22b. TELEPHONE (Include Area Code) (202) 767-4963 / 22c. OFFICE SYMBOL AFOSR/NC

DD Form 1473, JUN 86 — Previous editions are obsolete. — SECURITY CLASSIFICATION OF THIS PAGE

UNCLASSIFIED

abstract cont./ are produced with a much broader angular distribution and almost no population in either of the v" vibrational modes v"=1 and v"=2. We speculate that the higher energy methyl photofragments are the result of direct photodissociation at the surface: those with energies approaching 1.9 eV in concert with a ground state I atom, those with energies of about 1.1 eV in concert with a spin-orbit excited I* atom. Both of these channels are associated with photodissociation of methyl iodide molecules arranged perpendicular to the surface with the methyl end directed away from the surface. The lowest energy methyl photofragments, with translational energies of about 0.03 eV, result from the dissociation of methyl iodide molecules arranged with the methyl end directed toward the surface and scattered by the surface or undergoing multiple collisions with neighboring adsorbate molecules.

EXPERIMENTAL AND THEORETICAL INVESTIGATION OF SURFACE CHEMISTRY INDUCED BY DIRECT AND INDIRECT ELECTRONIC EXCITATION

Peter C. Stair and Eric Weitz
Department of Chemistry
Northwestern University
Evanston, Illinois 60208

August 1992

Final Report for August 1988 to January 1992
Contract Number: AFOSR-88-0297

DISTRIBUTION UNLIMITED

Prepared for

AIR FORCE OFFICE OF SCIENTIFIC RESEARCH
Bolling Air Force Base, D.C. 20332-6448

Abstract

A combined experimental and theoretical investigation of the photochemistry of methyl iodide (CD_3I) on TiO_2(110) (rutile) has been attempted in order to assess the importance of each of the possible direct or indirect photon absorption processes. We have used x-ray photoelectron spectroscopy (XPS), temperature programmed desorption (TPD) and a UHV chamber designed for 257-351 nm laser irradiation of the adlayer followed by time-of-flight mass spectrometry (TOF-MS). We have observed that following irradiation, CD_3 fragments are produced and ejected into the vacuum. These photofragments possess a characteristic translational energy distribution extending up to 1.9 eV (using 257 nm uv) but which varies somewhat with photodissociation energy and CD_3I coverage. Two broad peaks are visible in this distribution corresponding with CD_3 photofragments with translational energies of ~ 1.1 and ~ 0.03 eV. The higher energy fragments are produced with a relatively narrow angular distribution and possess some vibrational excitation in $v''=0$, 1 and 2, whilst those with low translational energy are produced with a broader angular distribution and mostly in the ground vibrational state $v''=0$. We speculate that the higher energy CD_3 fragments, translational energies approaching 1.9 eV, are from direct photodissociation of CD_3I molecules in concert with I atoms. Those with translational energies of ~ 1.1 eV correspond to CD_3 produced in concert with spin-orbit excited I^* atoms. Both channels are associated with CD_3I molecules arranged perpendicular to the surface with the methyl end directed *away* from the surface. The lowest energy fragments, with translational energies of ~ 0.03 eV, result from dissociation of CD_3I arranged with the methyl end directed *toward* the surface and scattered by the surface or within the adsorbate layer.

Introduction

Recently, there has been much activity in the field of surface-adsorbate photochemistry[1]. In particular, attention has been focussed on applying standard gas phase photochemistry techniques to probe gas-surface interactions. Much of the work has centered around the photochemistry of adsorbate molecules on metal surfaces.

This project is centered around a combined experimental and theoretical investigation of direct and indirect excitation of methyl-d_3 iodide molecules adsorbed on a TiO_2(110) (rutile) surface. It represents an attempt to elucidate the influence of the electronic structure of the substrate upon the photochemistry of an adsorbate molecule. Similar experiments have also been conducted in this laboratory using MgO(100) as a substrate[2,3,4]. MgO has a bulk electronic band-gap of 7.8 eV although a surface related feature has been observed at 6.1 eV[5]. Both of these values are larger than the energy of a 257 nm photon (4.83 eV) so electron-hole pair excitation is only possible at very short vacuum ultraviolet (vuv) wavelengths. However, TiO_2 has a bulk band-gap of ~ 3 eV[5,6] so only modest photon energies (≤ 410 nm) are needed to create substrate electronic excitation.

Such electronic effects may induce substantially different adsorbate photochemistry. Direct photon absorption by the adsorbate molecule can lead to prompt photodissociation in a similar fashion to the gaseous molecule. However, the close proximity of the surface or other neighboring molecules may significantly modify the potential energy surfaces of the adsorbate, and can result in (i) photodissociation modified by surface excitation (ii) photon induced reaction between adjacent adsorbate molecules (iii) substrate mediated desorption of an intact parent

molecule or (iv) adsorbate mediated photoejection of an intact parent molecule.

The first absorption band of methyl iodide, associated with promotion of a non-bonding p electron of the halogen atom to a σ^* orbital, extends from about 350 nm to shorter wavelengths and is maximum at 257.6 nm for CH_3I[7,8]. The absorption profile for CD_3I is very similar. Absorption results in direct C-I bond cleavage and the production of I atoms in either the ground ($^2P_{3/2} \equiv I$) or spin-orbit excited ($^2P_{1/2} \equiv I^*$) electronic state[9,10,11]. The overall branching ratio ($I^*/(I+I^*)$, is approximately 0.90 for CD_3I photolysis at 266 nm[12,13,14].

A detailed experimental program, in parallel with theoretical effort, has given us some insight into the important processes occurring at these surfaces, and we have been able to make comparisons between the photochemistry of CD_3I adsorbed on both "photoactive" TiO_2(110) and "photoinactive" MgO(100). The experimental work has been carried out under the supervision of Professors Peter Stair and Eric Weitz at Northwestern University and the theoretical work by Professors George Schatz of Northwestern and Robert Gerber of the Hebrew University in Jerusalem.

Experimental

(i) Outline of experimental scheme

A TiO_2(110) crystal, approximately 7x5x1 mm, was cemented to a Ni foil to which Ni support wires had been spot welded. The assembly was attached to a standard manipulator with facilities for liquid nitrogen cooling and heating by electron bombardment from a W filament mounted behind the Ni foil/TiO_2 crystal. Surface temperature was measured by a Chromel-Alumel thermocouple cemented to the edge of the crystal as close to the surface as possible. The surface was prepared by cycles of Ar^+ sputtering and subsequent annealing in $3x10^{-6}$ torr O_2 at 1000 K in an ultra-high vacuum (UHV) chamber (base pressure $3x10^{-11}$ torr). Work in this and other laboratories has shown that such a regime reproducibly generates clean, ordered and stoichiometric surfaces as examined by Auger electron spectroscopy (AES)[15], x-ray photoelectron spectroscopy (XPS)[16] and low energy electron diffraction (LEED)[17]. The surface prepared *in vacuo* by this method, was cooled to 100-110 K by contact with the manipulator liquid N_2 reservoir, and dosed with CD_3I by filling the UHV chamber to 10^{-9} to 10^{-6} torr CD_3I as appropriate. The exposure was calculated by integrating the ion gauge signal (approx 150 mm from the surface) over the dosing duration.

The adsorption behavior of CD_3I on TiO_2(110) has been investigated using TPD and XPS. Desorption experiments were performed using a multiplexed line-of-sight UTI 100C quadrupole mass spectrometer fitted with a 5 mm aperture and sampling masses corresponding to CD_3^+, I^+ and CD_3I^+ fragments. Similar results were obtained by using REMPI laser ionization of CD_3I and CD_3 coupled with time-of flight detection. During desorption, similar

signals were observed at masses 18 (CD_3^+), 127 (I^+) and 145 (CD_3^+I) amu indicative of parent fragmentation by the ionizing source following desorption. No evidence of dissociative adsorption or thermal dissociation was observed during TPD experiments.

XPS spectra of CD_3I on TiO_2(110) at 100-110 K have also been measured in a Vacuum Generators (VG) ESCALAB II/SIMSLAB spectrometer, equipped with a twin-anode Mg/Al x-ray source, a monochromated Al/Ag x-ray source and a 150 mm radius hemispherical energy analyzer. The chamber was also fitted with a uv transparent window which allowed irradiation of a 10x7x1 mm TiO_2(110) surface prepared as above. Irradiation experiments of a monolayer of CD_3I adsorbed on the TiO_2(110) surface were also performed in the VG ESCALAB vacuum chamber. The uv was provided by a 500 W low pressure Hg lamp fitted with a 10 cm pathlength cell filled with 0.25 M $NiSO_4$ to attenuate the ir output of the lamp. Interference filters were used to select certain uv wavelength regions corresponding to prominent Hg uv emission lines. Power output, measured at the lamp-to-sample distance (41 cm), was approximately 4 mW cm^{-2} using a 253.7 nm filter (bandwidth of 19 nm).

The experimental system used in photodissociation experiments, shown in Fig 1, has been described in detail elsewhere[2] but is outlined briefly here. The uv photodissociation source was provided by selecting a uv single line output from a high power Ar ion laser to produce uv at 351, 305 and 275 nm. Alternatively, by frequency doubling the 514 nm visible line by second harmonic generation (SHG) in a temperature controlled non-linear crystal we were able to generate uv at 257 nm. An acousto-optical modulator (AOM) was used to produce a variable duration uv pulse (>200 ns) from the cw beam. The beam, focussed to approximately 0.4 mm

diameter at the surface, intersected the sample at 45° from the surface normal. A half-wave plate allowed the photodissociation polarization to be rotated and was normally arranged so that the photon electric vector **E** was 45° (maximum) from the surface normal. Photolysis power measured at the entrance window to the UHV chamber was approximately 5-7 mW for 257 nm and up to 25 mW for the other wavelengths.

Photofragments produced as a result of irradiation of the methyl iodide adlayer were ionized by a second (probe) laser. Ionization selectivity is greatly increased if the probe laser wavelength is tuned to achieve resonance conditions. In much of the work presented here, methyl photofragments were ionized by a tunable uv probe laser with a focal point ~3 mm from the surface (directly over the photolysis area) *via* a resonantly enhanced multi-photon ionization (REMPI) technique. Resonant absorption of 2-photons prepares the CD_3 $3p\ ^2A_2''$ Rydberg state and subsequent absorption of a single photon results in promotion to the ionization continuum (2+1 REMPI). By changing the wavelength of the probe laser, different methyl vibrational states may be selectively ionized. The CD_3 radical in its ground vibrational state $v''=0$ is planar (D_{3h}), but at the uv probe wavelengths used in this work, it is also possible to access the first and second vibrationally excited states of the so-called "umbrella" mode $v''=1$ and $v''=2$ (out-of-plane H atom vibration).

The CD_3^+ ions created by the probe laser were detected by a time-of-flight mass spectrometry (TOF-MS) technique. Ions are accelerated by the first grid, labelled G1 in Fig 1 and also called the repeller, of a time-of-flight mass spectrometer biased positively (+100 to +1000 V) positioned 0.5-1 mm from the surface. Ions are then separated according to their charge-to-mass ratio q/m in a field-free region bounded by two grids at ground potential, G2 and

G3. Ions are counted by a three-stage micro-channel plate (MCP) detector.

Investigation using this experimental system has continued throughout the period covered by this report, however we have made significant improvements as detailed in the following sections.

(ii) Detection electronics

Improvements to the UHV system and peripheral equipment designed and completed during the term of this award have continued throughout. The most significant change has been concerned with the detector output signal processing.

In the original ion detection system, the output of the three-stage MCP was fed directly into a 100 gain Advanced Kinetics preamplifier and then into a LeCroy 9450 digital oscilloscope to collect an ion "time-of-flight" profile. The oscilloscope was used to average the preamplifier output over many probe beam shots as appropriate. However, charge fluctuations within the MCP assembly, caused "ringing" in the measured output signal; that is, damped charge oscillations after a true output pulse from the MCP. Fig 2 shows this phenomenon. The ringing oscillations significantly distorted the averaged time-of-flight profile, especially in complex or structured profiles. Additionally, during the collection of time-of-flight profiles with a very low absolute ion count, it was observed that single ions arriving at the detector produced MCP output pulses of widely different amplitude. Hence, averaging the total signal from each ion event over many shots could never give a true representation of the signal intensity (the total number of ions arriving in a particular time interval).

The acquisition an Ortec amplifier/discriminator, comprising a fast 200 gain preamplifier

and discriminator in a single unit, has allowed us to approach single ion counting. In this arrangement, the MCP output pulse is fed directly into the preamplifier/discriminator and assuming the amplified input signal is greater than the discriminator threshold, a 15 ns constant amplitude pulse is generated regardless of the input pulse amplitude. The output is then averaged over many probe shots as before, but in this way, the intensity at any part of the time-of-flight profile can be directly correlated to the number of ions detected in that arrival time interval since each discriminator pulse is equal in intensity and duration.

Ion counting has allowed us to extract considerably more information from typical experiments than using the original amplification electronics. In effect, it is possible to accurately record the arrival time of single ions arriving at the detector, and thus to count the number of ions in any time interval. The ultimate velocity/translational energy resolution at a particular repeller voltage is limited by the duration of the discriminator output.

(iii) Incorporation of angular information

In the initial experimental arrangement, the position of the probe beam focal point relative to the surface was determined by a moveable lens mounted inside the chamber. Usually, this was arranged to produce an ionization volume directly above the photolysis area and along the flight tube axis/surface normal. However, by changing the position of the probe focus, information about the angular distribution of the fragments can be obtained. Unfortunately, since the photolysis-ionization distance changes as the focus was moved, interpretation of results is non-trivial.

By mounting two quartz prisms on a rotatable flange at the point where the probe beam

enters the UHV chamber, we have been able to move the probe beam focus in an arc of +/-50° from the surface normal at approximately 8 mm from the photolysis area as shown in Fig 3. In this way, it was possible to collect methyl fragments ejected from the surface at a variety of angles from the surface normal whilst maintaining a constant photolysis-ionization distance. Thus, the problems associated with simple probe beam focus translation experiment were avoided.

Results

A. Adsorption behavior

In parallel with photolysis experiments, we have studied the adsorption behavior of methyl iodide on TiO_2(110) by other surface techniques.

(i) Temperature programmed desorption

The temperature of the maximum desorption rate ("desorption peak") for CD_3I on the 100 K TiO_2(110) surface, shows complex behavior, changing markedly with surface coverage. Representative TPD profiles are shown in Fig 4(a) to 4(d). At low exposures (less than 1.5 L), two desorption peaks are observed as shown in Fig 4(a). With increasing CD_3I exposure, the higher temperature peak, initially located at about 195 K, becomes more intense and decreases in desorption temperature. However, a noticeable high temperature "tail" remains, extending up to about 220 K. The lower temperature peak, at about 152 K, does not appear to change desorption temperature. After 1.5 L CD_3I exposure, the two peaks have merged to form a single peak which continues to decrease in desorption temperature to 153 K after exposure to 3.1 L CD_3I which we shall call the α phase. Exposures of more than 3.1 L results in the appearance of a separate β desorption peak at 132 K. This peak grows in intensity with CD_3I exposure, as shown in Fig 4(b) but remains centered at 132 K, although there is evidence for the persistence of the 153 K peak also. An exposure of greater than 6.9 L generates yet another higher temperature desorption peak, the γ phase as shown in Fig 4(c), centered at about 143 K. Loss of the 132 K peak occurs between 7.7 and about 11.5 L. Fig 4(d) shows a single γ desorption peak which persists up to the highest exposures of approximately 50 L, gradually increasing in

peak desorption temperature. At 38.2 L it is centered at 146 K.

The desorption data indicates several distinct coverage regimes for CD_3I on the $TiO_2(110)$ surface and may be interpreted according to a dipole interaction model. At the lowest coverages (< 1.5 L) there are two desorption peaks, one located at about 155 K which does not appear to change desorption temperature with coverage, and one initially located at about 195 K which shifts to lower desorption temperature with increasing coverage. The higher temperature peak has merged with the lower temperature peak after exposure to about 2 L and is located at 155 K after 3.1 L. These features, due to the first adsorbed CD_3I layer, are indicative of phase coexistence in the first layer. At high coverages (up to 3.1 L), only a single phase remains. Curiously, this feature does not appear to saturate as one would expect for completion of a monolayer, but this may be related to either the proximity of the α and β peaks (intensity "sharing") or alternatively, it may be that the second layer β peak, begins to form (at >3.1 L) before the first α layer is fully completed. The decreasing α peak desorption temperature with coverage suggests that repulsive interactions between neighboring adsorbate molecules become increasingly important, decreasing the molecular binding energy to the $TiO_2(110)$ surface.

At exposures greater than 3.1 L, the appearance of the β desorption peak due to the second layer is noted which persists up to about 6.9 L. Between about 6.7 and 11.5 L, the second layer desorption peak is gradually *replaced* by a higher temperature peak suggestive of a coverage dependant phase change taking place. It is important to note that between 7.7 and 10.5 L, we see loss of the β peak, not merely saturation: the γ peak grows with loss of the β peak. At exposures of 11.5 L or more, the increasing desorption peak temperature and the distinctive peak shape of zeroth-order kinetics expected for molecular desorption from

multilayers, is seen.

On the basis of the above, monolayer coverage was assumed to be at approximately 3.1 L, immediately prior to the appearance of the second layer β desorption peak. The exposure (in L) can be compared to surface coverage (in terms of monolayers) by calibrating with the total TPD intensity at each exposure. Fig 5 shows the increase in total flux measured at the mass spectrometer during desorption for exposures up to about 40 L. Guided by the desorption profiles of Fig 4, separate "fits" to the data are given for 0 to 3.1 L (up to 1 ML) and 3.1 L and above (greater than 1 ML). The figure shows a reasonably proportionate increase in desorbing CD_3I flux with CD_3I dose as will be discussed later.

(ii) X-ray photoelectron spectroscopy

Spectra show the binding energy of the C(1s) and the I(3d) peaks remain reasonably constant with coverage (at 285.3-285.5 eV and 620.3-620.7 eV respectively after correction for charging) indicative of molecular adsorption throughout the exposure range examined. As the exposure is increased, the I:$3d_{5/2}$ core level binding energy (BE) (the center of the peak at FWHM), as shown in Fig 6, shifts from 620.7 eV to 620.3 eV BE at 3.3 L (approximately 1.1 ML). In the exposure regime between 3.3 L and 8.2 L, the binding energy remains constant at 620.3 eV. This is the coverage regime where the second CD_3I layer forms. At greater exposures, the I($3d_{5/2}$) photoelectron peak shifts slightly to 620.5 eV BE and is constant thereafter with increased exposure. The C(1s) peak shows similar behavior although the adsorption of C containing molecules from the vacuum system during spectral accumulation was noted, causing a general broadening of the C(1s) peak.

It is also apparent from Fig 6, that the I(3d) intensity does not steadily increase with coverage. Instead, it rises almost linearly with CD_3I exposure, reaching a maximum at approximately 7.5-8.5 L and then falls abruptly, increasing much more slowly thereafter. The variation in the $I(3d_{5/2})$/Ti(2p) ratio with coverage is shown in Fig 7. It will be recalled that TPD data in this exposure region showed the growth of a low temperature desorption peak attributed to growth of the second and third layers. The replacement of this peak with a higher temperature desorption peak at 8-10 L corresponds to the sharp decrease seen in the $I(3d_{5/2})$/Ti(2p) ratio as measured by XPS.

The exact exposure required to observe the sharp fall in the $I(3d_{5/2})$/Ti(2p) ratio was observed to vary slightly although the general trend was very reproducible. In particular, the length of time between dosing and spectral accumulation, and the temperature of the $TiO_2(110)$ crystal was found to be important. The $I(3d_{5/2})$/Ti(2p) ratio was relatively constant with time for exposures less than about 7 L or for exposures greater than 9 L. However, the $I(3d_{5/2})$/Ti(2p) ratio was observed to decrease markedly with time for exposures in the regime 7-9 L with the sample held at 108 ± 3K throughout as shown in Fig 8. It seems reasonable to conclude that some sort of molecular rearrangement (phase change) takes place at these coverages.

B. Photodissociation

The majority of the work undertaken during this research period has been concerned with the 257 nm laser photodissociation of CD_3I, primarily at monolayer coverage, on the rutile surface. Some work has been conducted at other photolysis wavelengths and methyl iodide coverages. The uv photochemistry of CD_3I has also been investigated by XPS using a filtered

500W Hg lamp producing uv at 253 nm as discussed below.

(i) Adlayer compositional changes investigated by XPS.

The C(1s)/Ti(2p) and I($3d_{5/2}$)/Ti(2p) intensity ratios were determined after 253 nm Hg lamp irradiation of a 1.05 ML CD_3I adlayer on a clean TiO_2(110) surface held at $\leq$ 106 K. It is obvious from Fig 9, that there is a rapid decrease in both the C(1s)/Ti(2p) and I($3d_{5/2}$)/Ti(2p) intensity ratios, but the I($3d_{5/2}$)/Ti(2p) ratio falls more slowly with irradiation. The C(1s) peak intensity is reduced by half it's initial value in about 8 minutes, the I:3d in 24 minutes.

Irradiation of the adlayer causes the composition of the irradiated area to be changed: specifically, methyl species depletion occurs. It is possible to derive an effective cross-section for the removal of methyl species if it is assumed that the overall reaction is first order with respect to methyl concentration. In this case, the rate of methyl depletion is given by, $\ln\{[CD_3]_t/[CD_3]_0\} = \sigma_{253}\, n h\upsilon_t$ where $[CD_3]_t$ is the surface methyl concentration at time t, $[CD_3]_0$ is the initial surface methyl concentration, σ_{253} is the cross-section for methyl depletion at 257 nm and $nh\upsilon_t$ is the number of photons incident in time t. In this way we can estimate the cross-section for removal of C species as 3.2×10^{-19} cm^2 and for removal of I species as 1.1×10^{-19} cm^2.

The overall loss in both C and I species is accompanied by changes in the core level photoelectron peak shapes. As shown in Fig 10, the I($3d_{5/2}$) peak is initially centered at 620.3 eV binding energy but after 10 minutes uv irradiation, the peak has broadened considerably and shifted to lower binding energy suggesting the presence of a lower binding energy component. After 60 minutes irradiation the peak has moved to 619.0 eV BE and is narrower than those observed at intermediate irradiation durations. Similar, though less pronounced, changes occur

to the C(1s) peak shape as shown in Fig 11. It is initially located at 285.3 eV BE and shifts to 284.7 eV BE after 60 minutes of 253.7 nm illumination.

(ii) Photofragment identity following 257 nm laser irradiation

A typical time-of-flight (TOF) profile of gas phase CD_3I obtained by back-filling the UHV chamber is shown in Fig 12. The probe laser in this case was tuned to the 2+1 resonant absorption condition for ground state $CD_3 \rightarrow CD_3^+$ *via* the CD_3 $3p^2A_2''$ intermediate at $h\upsilon \simeq 333.75$ nm (29,950 cm^{-1}). It shows ions at flight times corresponding to production of CD_3I^+ (parent), I^+ and CD_3^+ (daughter) ions. At higher background pressures, very weak signals can be seen corresponding to CD_2^+, CD^+ and atomic C^+.

In contrast, a time-of-flight profile obtained from the subsequent ionization of photofragments produced by 257 nm irradiation of monolayer CD_3I adsorbed on $TiO_2(110)$ at 110 K, shown in Fig 13, clearly shows only ions corresponding to CD_3^+. Again, weak CD_2^+, CD^+ and C^+ signals were also observed, especially at very high methyl iodide coverages, the result of sequential C-D bond breaking in a similar way to that observed at shorter wavelengths[18,19]. Obviously, any significant parent desorption from the surface would generate CD_3I^+ and I^+ ion signals in a similar way to that observed for the gas phase molecule. Thus, it appears that photon induced parent desorption is minimal and we can assign a dissociation:desorption ratio of at least 100:1. In contrast, desorption of parent has been observed for the CH_3I on MgO(100) system[3]. In similar measurements, the photodissociation:photodesorption ratio in that work was found to be close to 4:1, representing a significant enhancement for desorption over $TiO_2(110)$. A full consideration is deferred until

the discussion section.

(iii) Velocity distribution of the methyl photofragments

In a time-of flight mass spectrometer with a single acceleration stage and a field-free region as used in the work presented here, the total ion flight time is given by

$$t_{arr} = \frac{\sqrt{v_z^2 + 2as} - v_z}{a} + \frac{D}{\sqrt{v_z^2 + 2as}} \qquad (1)$$

where v_z is the velocity component of the neutral fragment along the time-of-flight (z) axis, s is the distance between the ionization point and G2, D is the length of the field-free region, and $a = qE/m$ is the acceleration imparted to the ions if q/m is the charge to mass ratio and $E = V/d$ is the electric field strength. V is the potential difference and d the distance between G1 and G2 (see Fig 1). If a low potential is applied to G1, the velocity of the neutral prior to ionization is significant in determining the flight time. Neutral fragments having zero initial velocity component along the flight tube axis (ie $v_z=0$) will arrive at the detector at a time given by:

$$t_{arr}(v_z=0) = \frac{2s + D}{\sqrt{2as}} \qquad (2)$$

dependent only on the physical dimensions of the flight tube, the potential on G1 and the charge-to-mass ratio of the ion.

A typical CD_3^+ time-of-flight profile for monolayer CD_3I on $TiO_2(110)$, obtained with G1 = +100V and G2 = G3 = 0 V, is shown in Fig 14. Photodissociation pulse duration/delay

conditions were arranged to ionize methyl neutrals with initial velocities of 200-20000 ms^{-1}. Clearly it shows fragments are produced with a broad velocity distribution which contains two peaks centered at 600 and 3500 ms^{-1}. These velocities correspond to CD_3 translational energies E_{trans} of 0.03 and 1.08 eV respectively. It is important to note that methyl ions are observed with velocities up to about 4500 ms^{-1}, representing an E_{trans} of up to 1.88 eV. The apparent relative proportions of the photofragments cannot be inferred directly from such profiles since the CD_3 ionization probability is velocity dependant.

Many of these profiles have been taken for a variety of CD_3I coverages. Some of these are shown in Fig 15. The use of the ion counting detection electronics discussed above has allowed us to measure such a profile for exposures as small as 0.04 L (approximately 1/100th monolayer!). All coverages show the same general features. However, for exposure up to 1 ML, we note a slight increase in both the intensity and velocity of the high energy CD_3 photofragments. Upon exposure to multilayer doses, the intensity of the high energy CD_3 peak is very much reduced relative to the lower energy peak and it is also decreased in velocity to about 3300 ms^{-1}. A slight decrease in the low energy CD_3 peak velocity is also observed.

The TOF profiles suggest that the mechanism(s) responsible for producing this CD_3 velocity distribution is coverage dependent above 1 ML: the proportion of "slow" (500-1000 ms) to "fast" (3000-4000 ms^{-1}) CD_3 photofragments increases as the surface coverage is increased.

(iv) A cross-section for adsorbate photodissociation of CD_3I at 257 nm.

Assuming the loss of CD_3 and I from the CD_3I adlayer to be a first order process, the cross-section for removal of CD_3 species upon laser irradiation can be calculated in a similar

way to that given above. Hence by measuring the total methyl signal intensity as irradiation of the surface adlayer proceeds, as shown in Fig 16, it is possible to calculate σ_{257} (an overall cross-section for loss of methyl species). In this way, we calculate $\sigma_{257}=1.5\text{x}10^{-19}$ cm^2 for methyl removal at 257 nm from monolayer CD_3I adsorbed on the TiO_2(110). This compares favorably with the value for σ_{253} of $3.2\text{x}10^{-19}$ cm^2 calculated from the decay of C(1s) intensity measured by XPS after Hg lamp irradiation as indicated above.

Furthermore, by examining the decrease in signal intensity for each of the CD_3 velocities bands observed in the TOF profiles with G1 = +100 V, we were able tc determined σ_{257} with velocity selection. Thus, σ_{257} for methyl fragments of 200-2000 ms^{-1} ("slow") and 2000-20000 ms^{-1} ("fast") was determined to be $1.5\text{x}10^{-19}$ cm^2 in both cases. Obviously the overall cross-section for all fragments (200-20000 ms^{-1}) as quoted above, is also $1.5\text{x}10^{-19}$ cm^2.

(v) Methyl fragment angular distributions

Measurements of the angular distribution of methyl photofragments has indicated that, following CD_3I photodissociation at the surface, CD_3 is directed preferentially along the surface normal at all coverages. Fig 17 shows the variation in CD_3^+ intensity (measuring the 200-20,000 ms^{-1} ("total" velocity distribution measured with G1 = +1000 V) at multilayer coverage with the probe beam detecting CD_3 ejected along non-normal directions up to +/-50° from the time-of-flight tube axis. Unquestionably, methyl fragments are preferentially expelled along the direction of the surface normal. However, there is intensity detectable as far as 50° from the surface normal (probe beam rotation limit) and the distribution is generally broad.

Fig 17 also shows the similar angular distribution for multilayer CD_3I on TiO_2(110)

obtained with velocity selection made by varying the photolysis-probe delay and photolysis pulse duration to favor detection of a restricted methyl velocity range. It similarly demonstrates that, while there is a preference for methyl fragments of 200-20000 ms^{-1} ("total" intensity) to be directed along the surface normal, the effect is greatest for the fastest CD_3 fragments with velocities >2000 ms^{-1}.

Reduction of the G1 repeller voltage to allow velocity selection is not appropriate for off-normal CD_3^+ collection. In order to assess the validity of fragment angular information collected by rotating the probe beam in an arc around the photolysis area, computer simulations[20] of the methyl ion trajectories under a variety of experimental conditions were performed. In particular, the effect of methyl fragment initial energy (velocity), direction with respect to the surface normal, and flight tube potentials (acceleration conditions) was investigated. Some of the results of the simulations are shown in Figs 18 and 19. In particular, the simulations highlighted that with low potentials applied to G1 (<700 V) of the TOF-MS, high velocity CD_3 fragments would not reach the MCP detector. For this reason, the usual time-of-flight profiles obtained with 100 V on G1 were found to be truncated with respect to higher velocity ions at large off-normal angles and velocity selected angular measurements could not be performed in this way. For this reason, the data of Fig 17 was taken with G1 = 1000 V, the velocity selection being performed by varying the photolysis pulse duration and probe delay conditions.

(vi) Internal (vibrational) energy of methyl photofragments.

As mentioned above, by changing the probe laser wavelength it is possible to access vibrationally (and rotationally) excited states of the methyl radical. Fig 20 shows the CD_3^+ ion

signal ($\equiv$ 18amu) with changing probe laser wavelength following 257 nm photodissociation on a multilayer covered TiO_2(110) surface. The positions of the excited state resonances ($\upsilon''=0$, 1, 2 also referred to as 0_0^0, 2_1^1 and 2_2^2) are indicated and it clear that there is much more intensity in the ground state ($\upsilon''=0$ mode) than in either of the excited states. No intensity is visible in the $\upsilon''=3$ mode. Indeed, the relative excited state populations are, at first glance, less than for photodissociation of a supersonically cooled CD_3I molecular beam[12], or than photodissociation on the MgO(100) surface under similar experimental conditions[2] as will be discussed later. Unfortunately, it was not possible to obtain similar spectra from monolayer or submonolayer coverages due to the low absolute CD_3^+ flux produced by irradiation of low coverage surfaces.

It is also possible to measure the velocity distribution of each of the vibrationally excited states of the CD_3 by fixing the probe laser wavelength at the center of the excited state resonances. Time-of-flight profiles were thus taken for multilayer coverages (approximately 200 L exposure) with G1 = 100V to generate velocity information about the vibrationally excited methyl photofragments. These are shown in Fig 21. They clearly demonstrate that the low energy methyl fragments are predominantly produced with $\upsilon''=0$, ie no vibrational excitation. The higher energy methyl fragments possess a relatively large proportion of excitation in $\upsilon''=1$ and $\upsilon''=2$. The appearance of Fig 20 is therefore somewhat misleading since it represents the *overall* internal vibrational state distribution of CD_3 photofragments. It is dominated by the low vibrational state population characteristics of the lower energy CD_3 fragments, which predominate at multilayer coverages (see for example, Fig 15). The high energy CD_3 fragments appear to have a very different vibrational population.

(vii) Photodissociation at other wavelengths

We have recently undertaken a study of the photodissociation of monolayer CD_3I at wavelengths other than 257 nm. As mentioned above, other uv wavelengths are accessible using an Ar^+ laser by either single line selection optics or by frequency doubling. We have conducted initial experiments at both 275 and 305 nm which are still within the broad $\tilde{A}$ band absorption of CD_3I.

Time-of-flight profiles for 257, 275 and 305 nm irradiation of monolayer CD_3I on $TiO_2(110)$ at 100-110 K are shown in Fig 22 acquired under similar experimental conditions. While they essentially exhibit the same general features, several important differences can be noted. Firstly, the maximum CD_3 intensity ($\propto$ ion count) for 305 nm photolysis is much less than for 257 and 275 nm (after correction for different photolysis power densities at the surface). Secondly, the range of flight-times measured following 275 and 305 nm photodissociation is noticeably truncated compared to 257 nm; the methyl photofragment velocity distribution is narrower.

We have also been able to measure the decay of the CD_3 signal intensity as irradiation at these wavelengths proceeded to establish effective cross-sections for methyl removal as above. Velocity selection has allowed us to estimate σ_{275} and σ_{305} for both the high and low translational energy CD_3 photofragments (200-2000 and 2000-20000 ms^{-1} respectively). In these cases, for 275 nm incident radiation σ_{275}"fast" $=\sigma_{275}$"slow" $=\sigma_{275}$"total" $=3.1\times10^{-19}cm^2$ and for 305 nm incident radiation σ_{305}"fast" $=7.2\times10^{-20}cm^2$, σ_{305}"slow" $=9.5\times10^{-20}cm^2$ and thus σ_{305}"total" $=8.5\times10^{-20}cm^2$.

These values indicate that for the CD_3I adlayer, the absorption cross-section is greater

at 275 nm than at 257 nm. However, the gas phase absorption cross-section is reported to be maximal at ~260 nm[21] with a value of $1.3 \times 10^{-18} cm^{-2}$. Obviously, dissociation at the surface is accompanied by a reduction in absolute cross-section by more than an order of magnitude, possibly a consequence of quenching mechanisms, and is also somewhat absorption red shifted although without access to a more "tuneable" photolysis source, estimating this shift is difficult.

Fig 22 demonstrates a reduction of the mean E_{trans} for the high energy fragments as the photon energy is reduced. This is consistent with a mechanism where most of the available photon energy is channeled directly into the translational energy of the photodissociation products; ie, a direct dissociation event. Clearly, the maximum translational energy of the fragments must be related to the photon energy.

Discussion and Relation to Other Work

(i) The adsorption of CD_3I on $TiO_2(110)$

The work presented here on the adsorption of CD_3I on $TiO_2(110)$ at 100-110 K as investigated by TPD and XPS can be compared to other work on methyl halide adsorption. In particular, White *et al*[22] has studied the adsorption behavior of CH_3X (X=Cl, Br and I) on Ag(111) at about 100 K. In that work, two TPD peaks were observed at approximately 192 K and 136 K as due to monolayer and multilayer adsorption respectively. We have measured desorption temperatures of about 153 and 132 K respectively for CD_3I on $TiO_2(110)$ at 100 K. It is worth commenting that, as is expected, the multilayer desorption temperatures on the two substrates are not very different, but the desorption temperature of the monolayer peak is at considerably lower temperature for $TiO_2(110)$ implying a significantly reduced molecular binding energy. It is also worth noting that, for exposures up to 1 ML, White *et al* observed an *increasing* desorption peak temperature which he attributed to zero or fractional order desorption from 2D islands. We observe a decreasing peak temperature due to lateral repulsive interactions between isolated molecules. The appearance of the β phase peak is probably associated with second layer adsorption, although the continuing increase in intensity of the α peak may indicate that the second layer adsorption begins although the first layer is not complete.

While the molecular structure of the $(\alpha+\beta)$ phase(s) at 3.1→6.9 L in Fig 4 is unknown, it is clear that a slow molecular rearrangement takes place at exposures 6.9→10.5 L creating a multilayer γ phase which probably has a structure similar to the bulk methyl iodide crystal. The

existence of an intermediate (β) phase was not observed in the case of CH_3I on Ag(111). Further studies of this phenomenon are planned.

(i) Photodissociation

The choice of methyl iodide as a photolyzing molecule offers the chance of comparison to a large volume of relevant and comparable gas phase work performed to date. However, despite the large number of studies of REMPI and MPI of the gas phase CH_3I and CD_3I molecule, no coherent picture has emerged to satisfactorily explain the importance of the various multiphoton ionization pathways in methyl iodide and methyl-d_3 iodide.

It has been established that single photon absorption in methyl iodide causes excitation from the ground state $^2A_2$" $\tilde{X}$ to the $^2A_2$" $\tilde{A}$ band. Excitation is followed by prompt dissociation to create a methyl radical CH_3/CD_3 and either a ground state iodine atom, I $5^2P_{3/2}$ ($\equiv$I) or a spin-orbit excited iodine atom, I $5^2P_{1/2}$ ($\equiv$I*). At the probe laser wavelengths used in this study, further photon absorption causes resonant (2+1) ionization of the CD_3 radical $3p\ ^2A_2$"$\leftarrow 2p\ ^2A_2$" to produce CD_3^+. It has been speculated that the origin of the I^+ signals observed in TOF-MS of CH_3I/CD_3I at these and shorter wavelengths is a 2-photon non-resonant ionization of the I or I* atom from direct dissociation of the parent molecule[19,23,24]. However, we expect a very low probability for such non-resonant ionization, and it is more likely that I^+ signals arise from break-up of parent CH_3I^+/CD_3I^+. Powis and Black[25] noted similarities between the intensity behavior of the I^+ and CH_3/CD_3^+ ion signals with wavelength in the region 283-288 nm, also observed in the work of Gedanken *et al*[26], and the persistence of such signals over a relatively large wavelength range. This was attributed to parent absorptions which generate $CH_3I^+\backslash CD_3I^+$

ions by some MPI mechanism, which dissociate to produce charged daughter ions. Molecular ionization is also indicated in the ionization scheme of Bernstein *et al*[18], $CD_3I^+ \rightarrow CD_3 + I^+$. The fate of these excited parent ion states has not been investigated thoroughly to date. This mechanism does provide a explanation of the absence of I^+ signal from photodissociation at the $TiO_2(110)$ surface. If the I^+ ion is produced as a result of parent ion break-up, since very little parent ion desorption occurs from $TiO_2(110)$, this would necessarily also lead to an absence of I^+ signal.

According to the CD_3I energy level diagrams proposed[18,19,25,26], it can be seen that there are at least two possible ionization routes leading to the parent ion: one involving a 1-photon initial excitation to the $\tilde{A}$ state, the other an initial 2-photon absorption to the Rydberg $\tilde{B}$ state ($5p\pi \rightarrow 6p$ 16 states; all transitions from the $\tilde{X}\ ^2A_2''$ ground state are 2-photon allowed, though 4 of these states are 1-photon forbidden[26]). Indeed, the origin of parent ion observed in these photodissociation experiments has been a point of controversy.

The work of Bernstein on CH_3I[18] noted the production of *only* I^+ and CH_3^+ at all laser wavelengths between 266 and 307 nm. The authors explained the absence of CH_3I^+ by a lack of a direct 2-photon resonance route ($2 \times 266nm \equiv 9.32$ eV). The minimum ionization potential of CD_3I is 9.54 eV. In contrast, the work of Welge[19] using CD_3I at 266 nm showed all three ionic species, I^+, CD_3^+ and CD_3I in similar proportions to those observed here. It was suggested there that the appearance of parent ion was due to direct 2-photon excitation of *vibronically excited* CD_3I with energies of ≥ 1850 cm^{-1} ($\equiv 0.22eV \equiv 9.54$-9.32 eV) which at room temperature represents about 0.07% of the total CD_3I molecules. Power dependence measurements indicated the production of parent ion is a second order process at moderate probe

power densities. But, in the work presented here, with lower probe laser photon energies (3.72 eV), the vibronic excitation needed to account for appearance of CD_3I^+ in gas phase TOF-MS profiles according to the Welge mechanism, would be almost 1.3 eV!

On the basis of studies of CH_3I and CH_3I_n clusters, Vaida *et al* [27] has attempted to resolve the difference between the work of Berstein and Welge. Vaida discovered that with CH_3I molecular beam conditions set to produce only CH_3I monomers, CH_3^+ and I^+ were produced but no CH_3I^+. When beam conditions were set to produce dimers, I_2^+ was also seen (the result of sequential photodissociation events $CH_3I\text{-}IH_3C \rightarrow CH_3 + I\text{-}IH_3C \rightarrow CH_3 + I_2$). With very large clusters, only the CH_3I^+ ion was observed and attributed to "cage" effects where dissociation events are completely inhibited by the proximity of neighboring cluster molecules. Hence, it was speculated by Vaida that the CH_3I^+ ions seen by Welge, were due to cluster effects. Syage and coworkers[28,29] have also observed an absence of C-I photodissociation in large methyl iodide clusters.

Our TOF profiles show no evidence for large CD_3I clusters under any experimental conditions. Therefore, it is unlikely that the ionization of the CD_3I parent is due to cluster effects as proposed by Vaida. Additionally, the work where parent ion signals are *not* seen, are all concerned with CH_3I. The absorption bands of CD_3I may be sufficiently different to explain the appearance of parent ion in otherwise very similar experiments. We may also speculate that it is unlikely that CD_3I parent ionization also begins with 1-photon absorption to the $\tilde{A}$ state and subsequent 2-photon absorption to the ionization continuum, although this provides a maximum energy (at this wavelength) of 11.16 eV, more than needed to ionize CD_3I. Such a 3-photon process is probably relatively inefficient since the competing dissociation process from the $\tilde{A}$

state is very fast with a lifetime $\tau \leq 0.5$ ps[30].

It seems likely, at the probe wavelengths used here ($h\upsilon$=3.72 eV), that the origin of the parent ion is related to the proximity of a number of 2-photon resonant states (of CD_3I) in the $\tilde{B}\ ^2A_2'$ ($5p\pi \rightarrow 6p$) Rydberg band starting at 57,935 cm^{-1} (2x3.592 eV) and extending to 65,180 cm^{-1} (2x4.041 eV)[25]. It is envisaged that absorption of 2 photons by the ground state CD_3I molecule prepares one of the excited states in this band. Absorption of a further photon excites to the ionization continuum. If the initial 2-photon excitation is the overall rate-limiting step for this mechanism (excitation to the ionization continuum is "saturated"), the second order power dependance observed by Welge would apply.

It appears that we observe both excitation processes in our work, excitation to the $\tilde{A}$ state by a single photon followed by prompt dissociation to yield $CD_3+I^{(*)}$, and 2-photon excitation to the $\tilde{B}$ state which is then ionized by a further photon to yield CD_3I^+. Powis and Black[25], who similarly observed parent ion and both daughter ions for CD_3I and CH_3I photolysis between 283 and 287 nm, have commented that the duration and intensity of the photolysis pulse may determine the competitive balance between dissociation and ionization, short intense pulses favoring up-pumping to the molecular ion state.

(ii) Adsorbate photodissociation

The area of surface-adsorbate photochemistry has recently attracted intense interest and some progress has been made in establishing the important photochemical processes and assessing the influence of the surface. However, most of the systems showing photon driven chemistry studied to date have been centered upon diatomic and triatomic molecules adsorbed

on metal substrates, particularly Ag(111), Ni(111) and Pt(111). There have been some studies of alkyl halide photochemistry, but few concerned with semiconductor and insulator surfaces[1]. In almost all studies of adsorbed methyl halides using similar experimental techniques to those presented here, photodissociation is observed, regardless of the surface and coverage. In most cases, there is either direct or inferred evidence of expulsion of methyl photofragments following direct C-X bond cleavage. Methyl radicals are generated with non-Boltzmann velocity distributions and a generally lower translational energies E_{trans} than those observed for gaseous molecules.

Several authors, working with a variety of metal surfaces and alkyl halide adsorbates at a variety of uv wavelengths, have noted at least some retention of halide atoms and a fraction of the CH_3. This has been reported for CH_3Br on Ag(111)[31,32], Pt(111)[33,34,35,36,37] and Ru(001)[38] and for CH_3I on Ag(111)[39]. The XPS data in this study also shows a reduction in the C(1s) intensity with uv irradiation and a (smaller) reduction in the I(3d) total intensity. A shift in the $I(3d_{5/2})$ binding energy to 619.0 eV is consistent with reduction to an I containing cluster or molecular I_2 on the surface. The $I(3d_{5/2})$ binding energy for I_2 multilayers on Fe(100) has been measured as 619.3 eV BE[40], and as 619.9 eV BE for solid I_2[41]. TOF data indicates that I is not lost from the surface as CD_3I. Furthermore, XPS data has indicated that I is depleted at the surface more slowly than C, giving evidence that I is removed *via* some I-rich molecule, possible I_2. Experiments are planned to investigate the possibility of production of I-containing clusters and I_2 during uv irradiation.

The maximum expected translational energy E_{trans} of a CD_3 fragment produced in concert

with an I and I^* atom from 257 nm photodissociation of a gaseous CD_3I molecule, is expected to be 2.18 and 1.36 eV respectively. This is calculated by partitioning the 4.825 eV of the 257 nm photon according to simple momentum conservation arguments, assuming no vibrational/rotation excitation and dissociation energies $D_0(CD_3+I)=2.33$ eV and $D_0(CD_3+I^*)=3.275$ eV[13]. The difference in the dissociation energies obviously reflects the spin-orbit excitation, $E_{I^*}-E_I=0.945$ eV.

It is clear that the center of the high energy methyl band seen in our work, with methyl translational energies of about 1.1 eV, is similar to the expected maximum $E_{trans}=1.36$ eV (equivalent to $v=3800$ ms^{-1}) for production of CD_3 with spin-orbit excited state I^* atoms. The expected velocity for CD_3 corresponding to CD_3+I, with a maximum $E_{trans}=2.18$ eV, is 4800 ms^{-1}. By examining the TOF profiles of Figs 15 and 16, it is possible to observe some CD_3 ions with velocities approaching 4500 ms^{-1}, especially at close to monolayer coverages. Unfortunately, there is no clear peak in the velocity distribution above 4000 ms^{-1} which could confidently be associated with CD_3 from a CD_3+I dissociation event, and there are relatively few ions with $v>4000$ ms^{-1}.

Therefore, it is likely that CD_3 photofragments produced at the surface with initial velocities of approximately 3400 ms^{-1} originate from a dissociation event producing CD_3+I^*. The fewer fragments with velocities extending up to 4500 ms^{-1} originate from a dissociation event producing CD_3+I. It also appears that adsorbate photodissociation strongly favors the CD_3+I^* channel. The $I^*/(I+I^*)$ branching ratio is qualitatively similar to the 0.90 quoted overall branching ratio $(I^*/(I+I^*)$ for gaseous CD_3I photolysis at 266 nm[12,13,14]. The exact value was shown to be very dependant on the vibrational excitation in the $\upsilon^{"}$ mode of the CD_3 fragment.

Values of >0.95, 0.92, 0.8 and 0.57 have been quoted for $v''=0$, 1, 2 and 3 respectively[12]. Unfortunately, we are unable to calculate a value for the surface branching ratio, since the CD_3 ionization probability is a function of fragment velocity, but it appears qualitatively similar to gas phase dissociation, strongly favoring the I^* channel.

For the higher energy methyl photofragments ($v>2000$ ms^{-1}), the most probable CD_3 photofragment translational energy is less than the maximum calculated translational energy for each of the dissociation channels. Fig 18 has already indicated that these methyl photofragments possess a high proportion of vibrational energy in $v''=1$ and 2. The CD_3 produced with E_{trans} between ~ 1.1 and ~ 1.9 eV, due to direct dissociation of the CD_3I molecule at the surface to give CD_3 with I and I^*, generates vibrationally excited CD_3 with population in $v''=0$, 1 and 2. The population of the $v''=0$ mode is greatest, with less in $v''=1$ and 2 in accordance with the vibrational populations obtained for 266 nm dissociation of gaseous CD_3I by Houston *et al*[12] but different to those of Van Veen *et al*[13] whose work gave maximum population at $v''=2$ for the I^* branch and $v''=5$ for the I branch. Powis and Black[42] measured populations $v''=1>v''=2=v''=0$ for the I^* channel and $v''=1>v''=2>v''=0$ for the I channel using ~ 280 nm radiation to dissociate CH_3I.

The low velocity CD_3 fragments ($v<2000$ ms^{-1}) are mostly formed in $v''=0$. Furthermore, the small proportion of very low energy fragments ($E_{trans}\sim 0.03$ eV) which are formed in $v''=1$, seem to have a higher mean velocity, at around 1500 ms^{-1}, than those produced in $v''=0$. The origin of the intense, very low energy, vibrationally cool CD_3 fragments is probably associated with direct photoproducts which have undergone energy loss (both vibrational and translational) *via* collisional events with either the surface or neighboring

adsorbate molecules. Again, it is difficult to comment upon the proportions of direct and scattered CD_3 without knowing the ionization probability of different velocity CD_3 fragments. The angular distributions of each of the methyl velocity components also provides support that the low energy fragments are due to collisional events. The angular distribution for the high energy methyl fragments ($v > 2000$ ms^{-1}) is relatively narrow (approximately $\cos\theta^n$ where $n \simeq 15$) but the overall distribution ($200 < v < 20000$ ms^{-1}) is much broader with $n \simeq 5$. This implies a similarly broad angular distribution for the very low energy fragments ($v < 2000$ ms^{-1}). Collision and scattering of CD_3 created at some depth in the adlayer would be expected to broaden the angular distribution of methyl photofragments escaping into the vacuum. Similar $\cos\theta^n$ variations in methyl angular distribution were also obtained for CD_3I/CH_3I on the MgO(100) surface (with $n \simeq 4$) in this laboratory[4] and for multilayers CH_3Br on LiF(001)[43] (with $n \simeq 5$). Both of these experiments sampled the *total* methyl velocity angular distribution, which may be very different from the angular distributions of "fast" and "slow" methyl photofragments as measured in our work.

The origin of the low energy methyl photofragments has been speculated for some time based upon a model of the adsorption geometry of methyl halides on several surfaces. Recently, He diffraction results for CH_3Br on an LiF(001) surface[44] have confirmed that an incommensurate, ordered and aligned overlayer can be formed on LiF(001) (at 35K), with the C-Br bond axis normal to the surface alternating with CH_3 upwards/Br upwards. Obviously, the anti-parallel arrangement of CH_3Br molecules will produce both "direct" (methyl end away from surface) and "scattered" (methyl end towards surface) methyl fragments after a C-Br dissociation event. It is suggested here, that a similar anti-parallel packing geometry for CD_3I on the

$TiO_2(110)$ surface, will lead to a similar direct and scattered photodissociation products.

Our work is in good qualitative agreement with much of the work on adsorbed CH_3Cl and CH_3Br on surfaces. Arguably the most directly comparable work to the that presented here has been by Bourdon *et al*[43,45] on the 222 nm photodissociation of CH_3Br adsorbed on an annealed LiF(001) surface where CH_3 with a narrow E_{trans} distribution centered about 1.5 eV, and a broader E_{trans} extending down to around 0.1 eV, was observed. The 222 nm photodissociation of gas phase CH_3Br yields methyl fragments with mean E_{trans} of approximately 1.7 (corresponding to production of CH_3+Br^*) and 2.1 eV (corresponding to production of CH_3+Br)[46]. Furthermore, the energy of the 1.5 eV peak was observed to decrease by about 0.3 eV with increasing CH_3Br coverage (CH_3Br "ice"). Bourdon also noted a very intense, low CH_3 E_{trans} of about 0.3 eV for a rough (unannealed) LiF(001) surface. They attributed this to CH_3Br adsorbed at a variety of defect sites on the surface with stronger coupling of the adsorbate to a defect site.

It may also be argued that defects on the $TiO_2(110)$ surface are responsible for the very intense low energy methyl signal seen in this work. Indeed, it has been postulated that defect sites are an intrinsic part of surface reconstruction in the $TiO_2(110)$ surface. However, the increase in intensity of this low energy methyl peak with CD_3I coverage, suggests that it can also result from loss of translational energy by CD_3 by collision with other adsorbate molecules and is not controlled directly by the TiO_2 surface at such coverages. Only those methyl fragments produced at the very outermost part of the adlayer in thicker layers will still escape with no collisional losses. As the adsorbate layer becomes thicker, an increasing proportion loose energy during transport to the vacuum. As in our work, Bourdon *et al* were similarly not able to clearly

resolve two distinct high methyl velocities attributable to production of X and X^* atoms as observed in the gas phase and as has been observed for CH_3I on LiF(001)[47], although the authors comment that this was probably due to experimental limitations. Alternatively, a surface Br/Br^* branching ratio which greatly favors the Br^* channel would produce similar features. Time-of-flight profiles for methyl photofragments produced by irradiating CH_3Br multilayers on GaAs(110) with 193 and 248 nm radiation also show two distinct peaks in the velocity distribution[48]. Again, the fastest peak was assigned as due to direct photodissociation in the outermost layer, whilst the more intense low velocity peak was due to scattering of methyl photofragments produced deeper within the adlayer.

Photodesorption of intact parent alkyl halides has also been observed for CH_3Br on LiF(001) using 193 nm radiation[49], CH_3Cl on GaAs(100) at 193 and 248 nm[50], CH_3I on LiF(001) at 266 nm[47] and in this laboratory for CD_3I/CH_3I on MgO(100) at 257 nm[3]. Curiously, in the present work we have observed relatively little parent desorption. Proposed mechanisms to account for observed photodesorption from LiF(001), which is transparent to uv, include thermal desorption due to a rapid localized surface temperature rise as uv energy is deposited there[49,51] and a photoacoustical disturbance caused by absorption at F-centers in the crystal bulk[52]. In metals and semiconductors like TiO_2, the substrate is no longer transparent to uv and there is the possibility of band-gap excitation. Photodesorption of the intact adsorbate molecule is seen in the majority of instances of adsorption on semiconductors and metals. Most of the desorption observed from these materials has been attributed to some sort of charge-transfer mechanism following band-gap excitation[53]. It is therefore puzzling that there appears to be very little photodesorption of parent from the $TiO_2(110)$ surface even though there is the potential for "hot"

electron production at all the wavelengths used in this study. If it can be assumed that photodesorption follows excitation of the adsorbate-surface complex to some repulsive state, it appears that TiO_2(110) provides more efficient quenching mechanisms for the excited CD_3I-surface complex than MgO(100). These de-excitation mechanism's dissipate the photon energy (257 nm ≡ 4.82eV) via coupling to electronic/vibrational modes of the surface.

Conclusions

The work undertaken during the period of this contract has demonstrated uv photochemistry of CD_3I on the $TiO_2(110)$ surface. It has produced very interesting results and has given us important information about surface photochemical processes.

The adsorption of CD_3I on $TiO_2(110)$ shows curious adsorption behavior, as observed by TPD and XPS in the coverage regime approaching 2-3 monolayers. We have been able to demonstrate that, following photodissociation on the surface, methyl groups are expelled and a larger proportion of the I remains as I_2-like species as examined by XPS.

We have followed the photochemistry in detail using laser techniques. The employment of ion counting electronics in TOF-MS has meant that we have been able to clearly identify a methyl fragment velocity distribution after photolysis of CD_3I at several uv wavelengths. There are at least two distinct methyl fragment velocities at all coverages with broad translational energy distributions centered at approximately 1.1 (3500 ms^{-1}) and 0.03 eV (600 ms^{-1}). Some fragments are observed with translational energies of up to 1.9 eV. The high energy methyl photofragments are produced with significant population in $v''=1$ and 2 along the surface normal, while the low energy photofragments are produced mostly in the $v''=0$ state and have a broader angular distribution. In addition, the increased detection sensitivity has allowed us to assign an upper limit to the ratio of CD_3I dissociation to desorption at greater than 100:1. Under similar conditions, the dissociation/desorption ratio for CD_3I on MgO was significantly different at approximately 4:1.

We speculate that the high energy CD_3 is produced as a result of direct dissociation at

the outermost part of the adlayer in conjunction with spin-orbit excited I^* atoms. The low energy CD_3 is due to inelastic scattering/collisional events in the adlayer or at the surface. There is also evidence for CD_3 with translational energies up to 1.9 eV due to production of CD_3 with ground state I atoms. Scattering is expected to occur at all coverages due to the anti-parallel packing arrangement of alkyl halides in these adlayers.

Personnel

Principal Investigators:	Professor Peter C. Stair Professor Eric Weitz
Senior Investigators:	Professor Robert B. Gerber (Hebrew University) Professor George C. Schatz
Postdoctoral Research Associates:	Simon J. Garrett Tuwon Chang Maureen McCarthy (Hebrew University)
Graduate Students:	Victor P. Holbert

Publications

(1) Quantum theory of the photodissociation of IBr adsorbed on an MgO(100) surface.
M.I. McCarthy, R.B. Gerber and M. Shapiro
J. Chem. Phys. 92 (1990) 7708

(2) Molecular-dynamics simulations of the photodissociation of ICl adsorbed on a MgO(100) surface.
M.I. McCarthy and R.B. Gerber
J. Chem. Phys. 93 (1990) 887

(3) Photodissociation dynamics of CH_3I adsorbed on an MgO(100) surface: theory and experiment.
M.I. McCarthy, R.B. Gerber, K.A. Trentelman, P.G. Strupp, D.H. Fairbrother, P.C. Stair and E. Weitz, J. Chem. Phys., accepted for publication.

(4) An investigation of the adsorption of CD_3I on $TiO_2(110)$: XPS and TPD results.
S.J. Garrett, V.P. Holbert, P.C. Stair and E. Weitz, in preparation

(5) The 257-nm photolysis of CD_3I on $TiO_2(110)$: an examination of the methyl fragment.
S.J. Garrett, V.P. Holbert, P.C. Stair and E. Weitz, in preparation

Presentations

(1) The photochemistry of adsorbed small molecules: the 257-nm photolysis of CH_3I on $TiO_2(110)$.
S.J. Garrett, V.P. Holbert, P.C. Stair and E. Weitz
Gordon Conference "Dynamics of Gas-Surface Interaction", Andover, NH, August 1991.

References

1 For a recent review see X.L. Zhou, X.Y. Zhu, J.M. White, Surf. Sci. Rep. **13** (1991) 73

2 K.A. Trentelman, D.H. Fairbrother, P.C. Stair, P.G. Strupp, E. Weitz, J. Vac. Sci. Technol. A **9** (1991) 1820

3 K.A. Trentelman, D.H. Fairbrother, P.G. Strupp, P.C. Stair, E. Weitz, J. Chem. Phys. **96** (1992) 9221

4 D.H. Fairbrother, K.A. Trentelman, P.G. Strupp, P.C. Stair, E. Weitz, J. Vac. Sci. Technol. A, **10** (1992) 2243

5 V.E. Henrich, Prog. Surf. Sci. **9** (1979) 143

6 V.E. Henrich, Prog. Surf. Sci. **14** (1983) 175

7 D. Porret, C.F. Goodeve, Trans. Faraday Soc. **33** (1937) 690

8 M. Ito, P.C. Huang, E.M. Kosower, Trans. Faraday Soc. **57** (1961) 1662

9 T. Donohue, J.R. Wiesenfeld, J. Chem. Phys. **63** (1975) 3130

10 T.F. Hunter, K.S. Kristjansson, Chem. Phys. Lett. **58** (1978)

11 H.W. Herman, S.R. Leone, J. Chem. Phys. **76** (1982) 4759, 4766

12 R.O. Loo, H.P. Haerri, G.E. Hall, P.L. Houston, J. Chem. Phys. **90** (1990) 4222

13 G.N.A. Van Veen, T. Baller, A.E. De Vries, N.J.A. Van Veen, Chem. Phys. **87** (1984) 405

14 S.M. Penn, C.C. Hayden, K.J. Carlson Muysken, F.F. Crim, J. Chem. Phys. **89** (1988) 2909

15 for example N.R. Armstrong, R.K. Quinn, Surf. Sci. **67** (1977) 451

16 for example W. Gopel, G. Rocker, R. Feierabend, Phys. Rev. B: Condens. Matter, **28** (1983) 3427

17 for example L.E. Firment, Surf. Sci. **116** (1982) 205

18 Y. Jiang, M.R. Giorgi-Arnazzi, R.B. Berstein, Chem. Phys. **106** (1986) 17

19 J. Danon, H. Zacharias, H. Rottke, K.H. Welge, J. Chem. Phys. **76** (1982) 2399

20 Using the program "Simion PC/PS2", D.A. Dahl, J.E. Delmore, Idaho National Engineering Laboratory, 1988

21 D. Porrett, C.F. Goodeve, Proc. R. Soc. London Ser. A **165** (1938) 31

22 X.L. Zhou, F. Solymosi, P.M. Blass, K.C. Cannon, J.M. White, Surf. Sci. **219** (1989) 294

23 J.W. Hudgens, T.G. DiGiuseppe, M.C. Lin, J. Chem. Phys. **79** (1983) 571

24 D.H. Parker, Z.W. Wang, M.H.M. Janssen, D.W. Chandler, J. Chem. Phys. **90** (1989) 60

25 J.F. Black, I. Powis, Chem. Phys. Lett. **148** (1988) 479

26 A. Gedanken, M.B. Robin, Y. Yafet, J. Chem. Phys. **76** (1982) 4798

27 S.P. Sapers, V. Vaida, R. Naaman, J. Chem. Phys. **88** (1988) 3638

28 J.A. Syage, J. Chem. Phys. **92** (1990) 1804

29 J.A. Syage, J. Steadman, Chem. Phys. Lett. **166** (1990) 159

30 J.L. Knee, L.R. Khundkar, A.H. Zewail, J. Chem. Phys. **83** (1985) 1996

31 X.L. Zhou, J.M. White, Surf. Sci. **241** (1991) 259

32 X.L. Zhou, J.M. White, Chem. Phys. Lett. **167** (1990) 205

33 S.A Costello, B. Roop, Z.M. Liu, J.M. White, J. Phys. Chem. **92** (1988) 1019

34 Y. Zhou, W.M. Feng, M.A. Henderson, B. Roop, J.M. White, J. Am. Chem. Soc. **110** (1988) 4447

35 Z.M. Liu, S.A. Costello, B. Roop, S.R. Coon, S. Akhter, J.M. White, J. Phys. Chem. **93** (1989) 7681

36 G. Radhakrishnan, W. Stenzel, H. Conrad, A.M. Bradshaw, Appl. Surf. Sci. **46** (1990) 36

37 B. Roop, K.G. Lloyd, S.A. Costello, A. Campion, J.M. White, J. Chem. Phys. **91** (1989) 5103

38 B. Roop, Y. Zhou, Z.M. Liu, M.A. Henderson, K.G. Lloyd, A. Campion, J.M. White, J. Vac. Sci. Technol. A **7** (1989) 2121

39 X.L. Zhou, J.M. White, Surf. Sci. **241** (1991) 270

40 S.B. DiCenzo, G.K. Wertheim, D.N.E. Buchanan, Phys. Rev. B, **30** (1984) 553

41 P.M.A. Sherwood, J. Chem. Soc. Faraday Trans. **72** (1976) 1805

42 J.F. Black, I. Powis, Chem. Phys. **125** (1988) 375

43 E.B.D. Bourdon, P. Das, I. Harrison, J.C. Polanyi, J. Segner, C.D. Stanners, R.J. Williams, P.A. Young, Faraday Disc. Chem. Soc. **82** (1986) 343

44 G.N. Robinson, N. Camillone, P.A. Rowntree, G. Liu, J. Wang, G. Scoles, J. Chem. Phys. **96** (1992) 9212

45 E.B.D. Bourdon, J.P. Cowin, I. Harrison, J.C. Polanyi, J. Segner, C.D. Stanners, P.A. Young, J. Phys. Chem. **88** (1984) 6100

46 G.N.A. Van Veen, T. Baller, A.E. DeVries, Chem. Phys. **92** (1985) 59

47 J. Kutzner, G. Lindeke, K.H. Welge, D. Feldman, J. Chem. Phys. **90** (1989) 548

48 W.N. Schwarz, Q.Y. Yang, D.L. Chen, B.M. Osgood, J. Chem. Phys. **97** (1992) 722

49 F.L Tabares, E.P. Marsh, G.A. Bach, J.P. Cowin, J. Chem. Phys. **86** (1987) 738

50 M.R. Schneider, C.P. Dehnbostel, T.L. Gilton, J.P. Cowin, J. Appl. Phys. Submitted

51 K. Domen, T.J. Chuang, J. Chem. Phys. **90** (1989) 3318

52 I. Harrison, J.C. Polanyi, P.A. Young, J. Chem. Phys. **89** (1988) 1475

53 J.C. Polanyi, H. Rieley in "Dynamics of Gas-Surface Interactions", Royal Society of Chemistry Publ., 1991

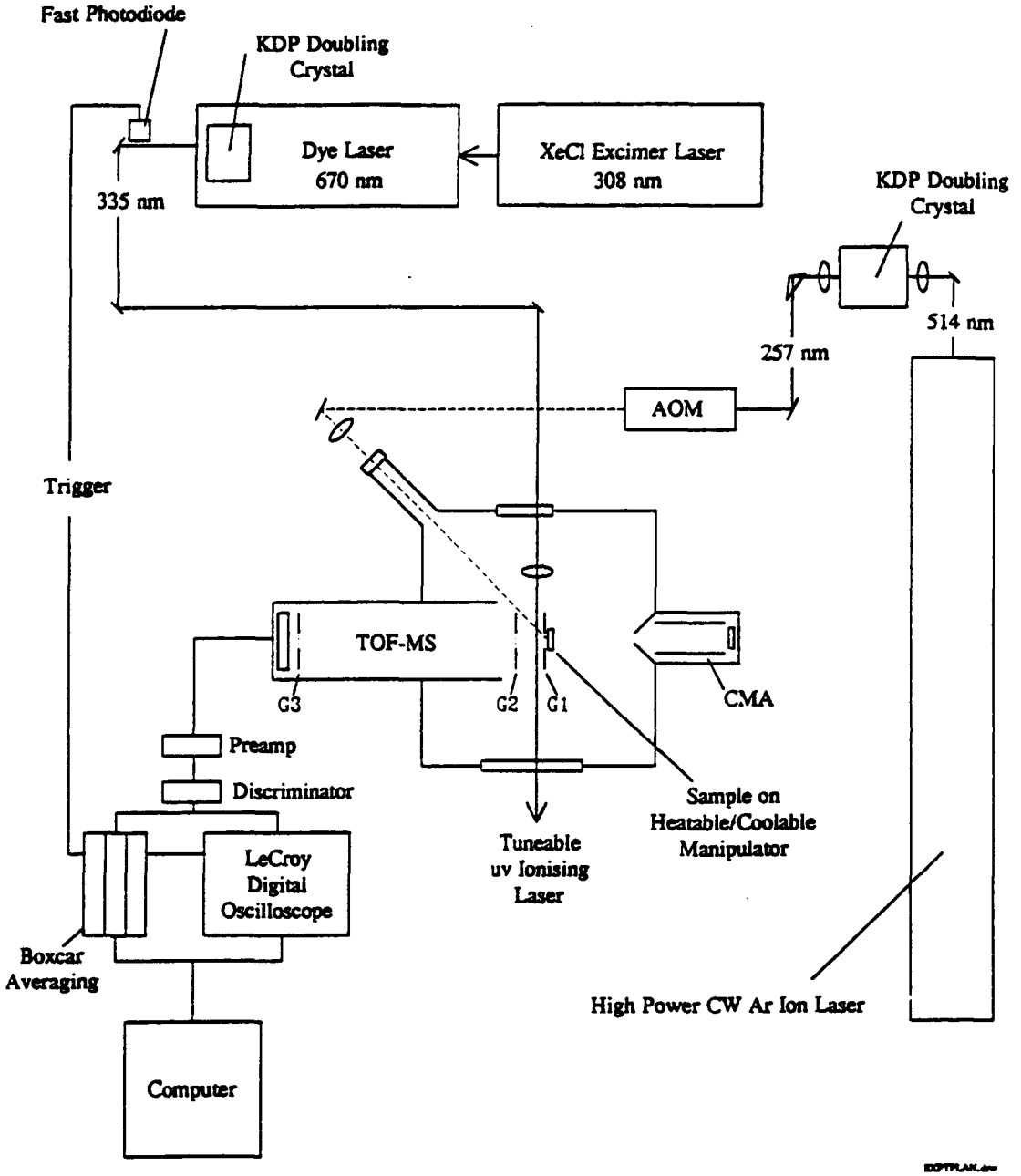

Fig 1: Schematic diagram of the UHV chamber/2 laser system used in surface photodissociation studies. The TOF-MS grids are shown as G1, G2 and G3.

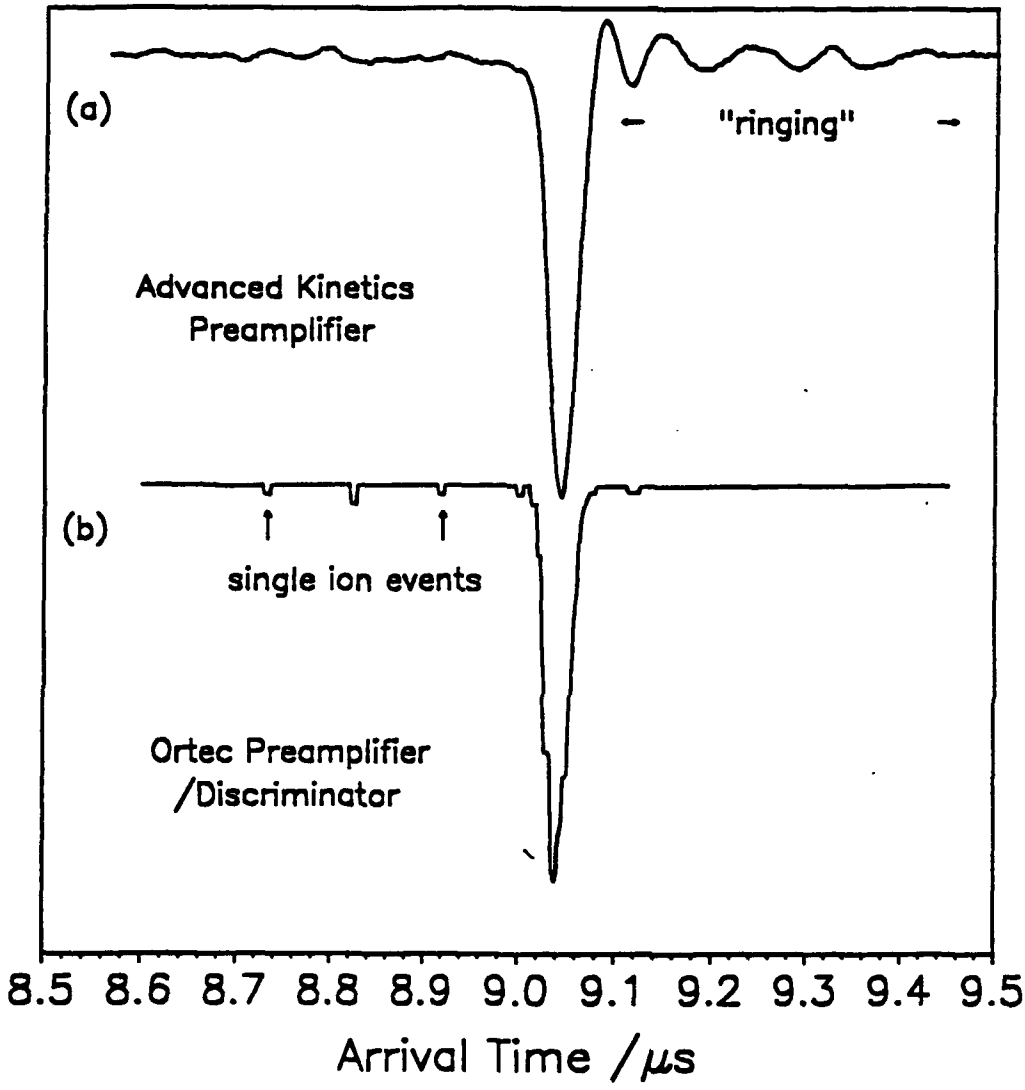

Fig 2: Typical TOF profiles for arrival times corresponding to CD_3^+ measured for gas phase photodissociation of CD_3I and G1 = 100 V. The CD_3^+ ion signal for both the original AK and recently acquired Ortec preamplifier/discriminator is shown.

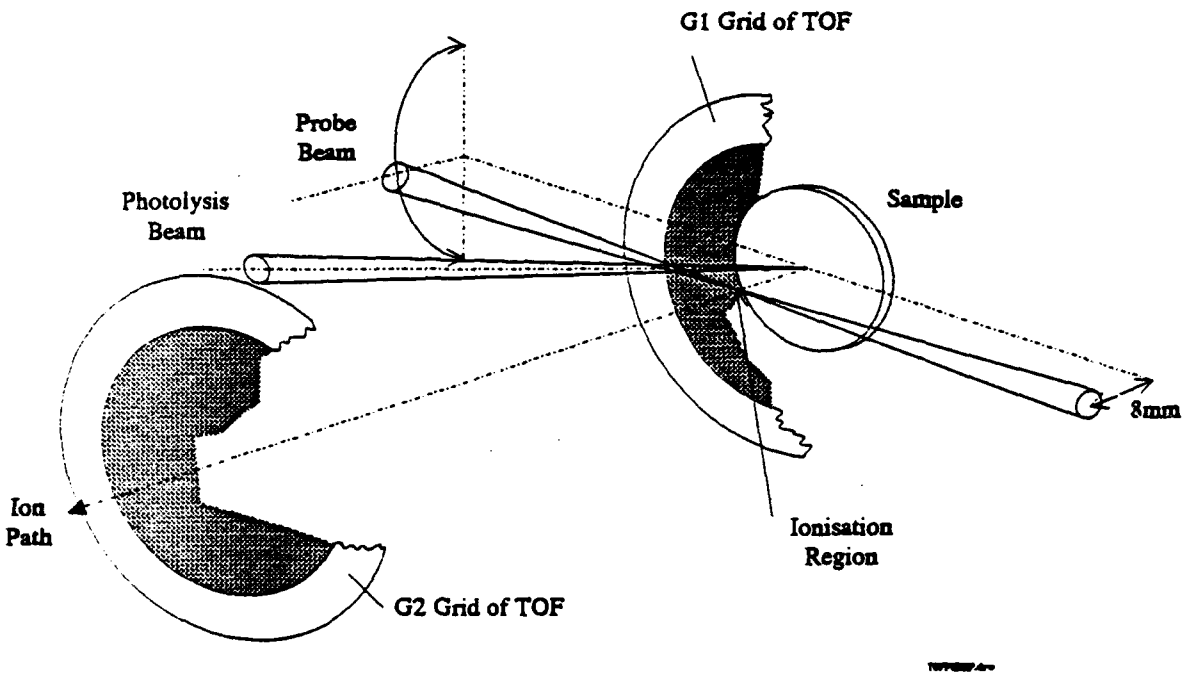

Fig 3: Diagram of TOF apparatus showing the geometry of the probe beam rotation used in methyl angular distribution experiments.

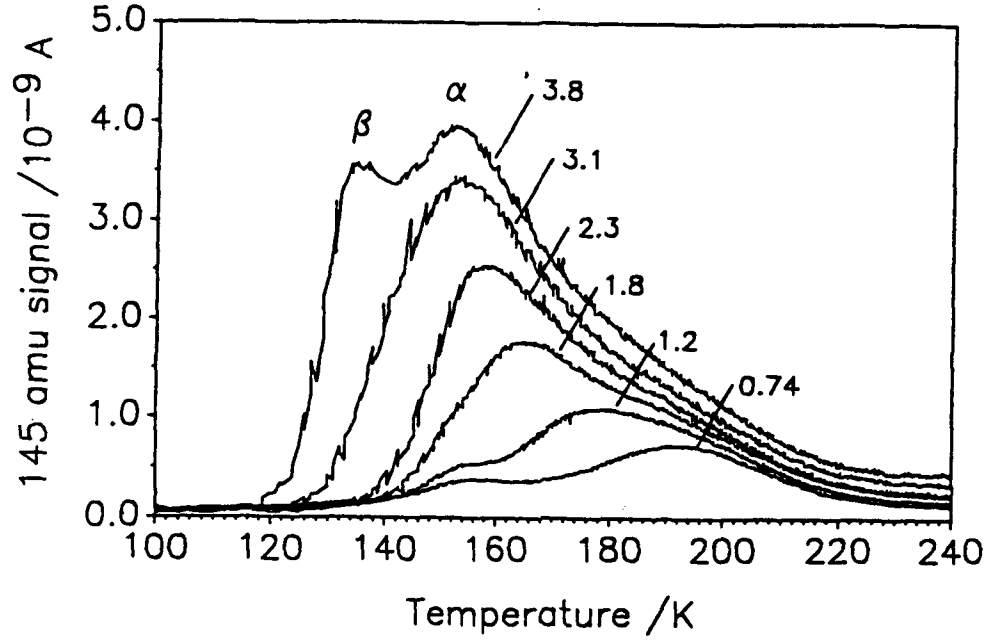

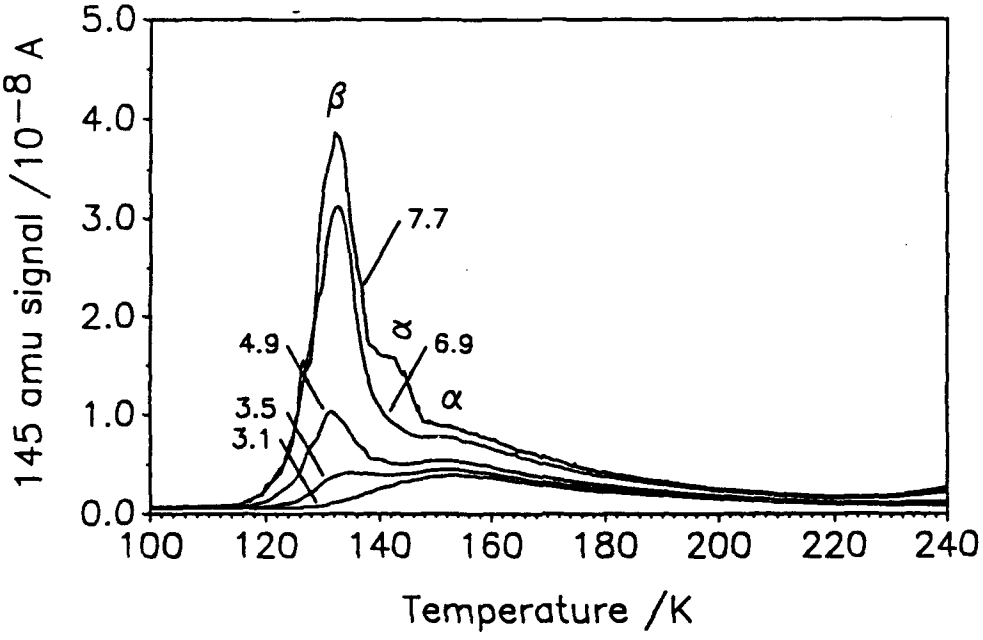

Fig 4(a)(Upper panel): TPD curves for CD_3I on $TiO_2(110)$ adsorbed at 100 K. Exposures up to 3.8 L show growth of an α and β desorption peak. Surface heating rate approximately 2.5 Ks^{-1}.

Fig 4(b)(Lower panel): TPD curves for CD_3I on $TiO_2(110)$ adsorbed at 100 K. Exposures between 3.1 and 7.7 L show the growth of the β desorption peak.

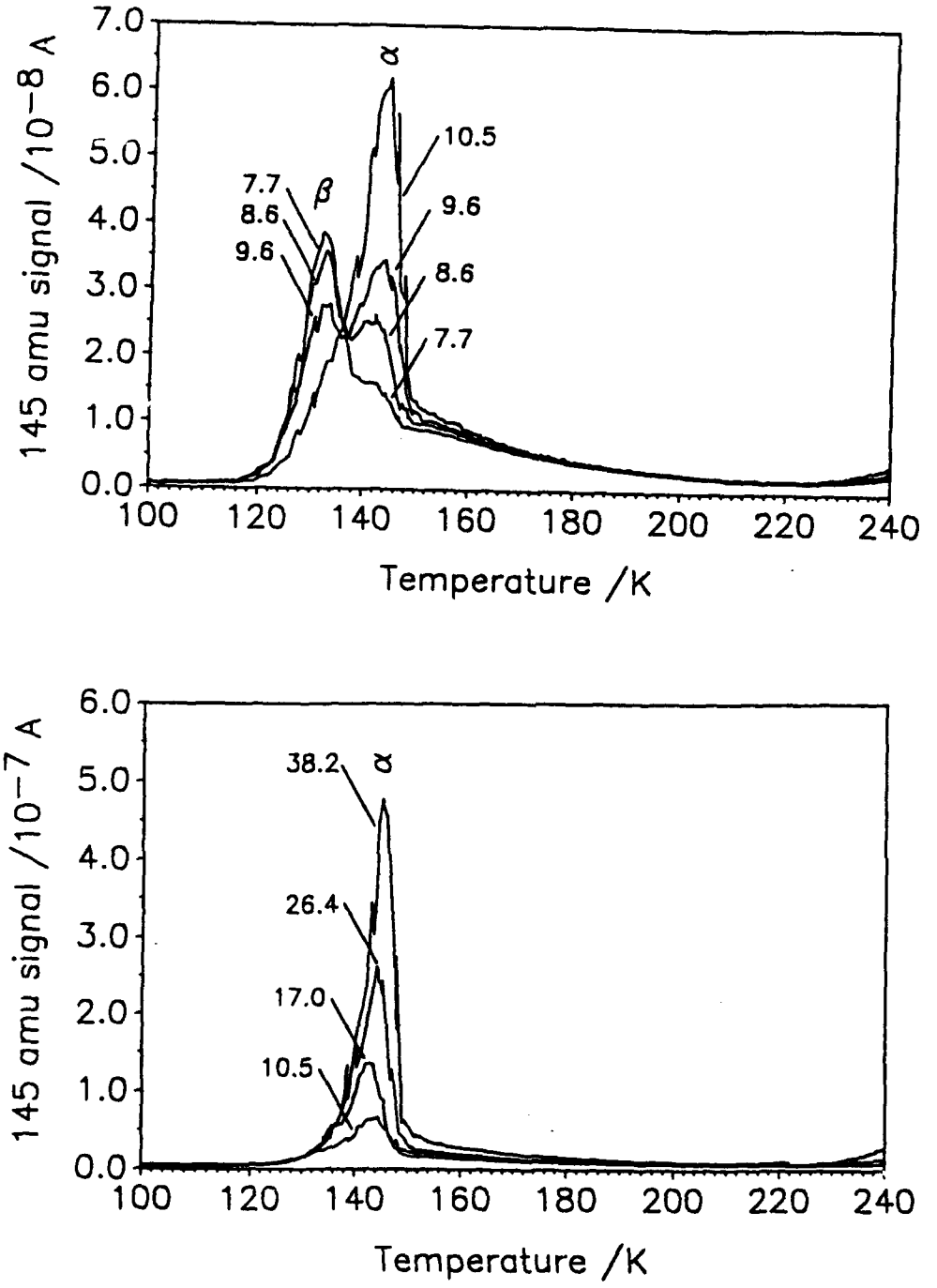

Fig 4(c)(Upper panel): TPD curves for CD_3I on $TiO_2(110)$ adsorbed at 100 K. Exposures between 7.7 and 10.5 L show loss of the β desorption peak, being replaced by a higher temperature γ peak.

Fig 4(d)(Lower panel): TPD curves for CD_3I on $TiO_2(110)$ adsorbed at 100 K. Exposures between 10.5 and 38.2 L show growth of the γ desorption peak due to multilayers.

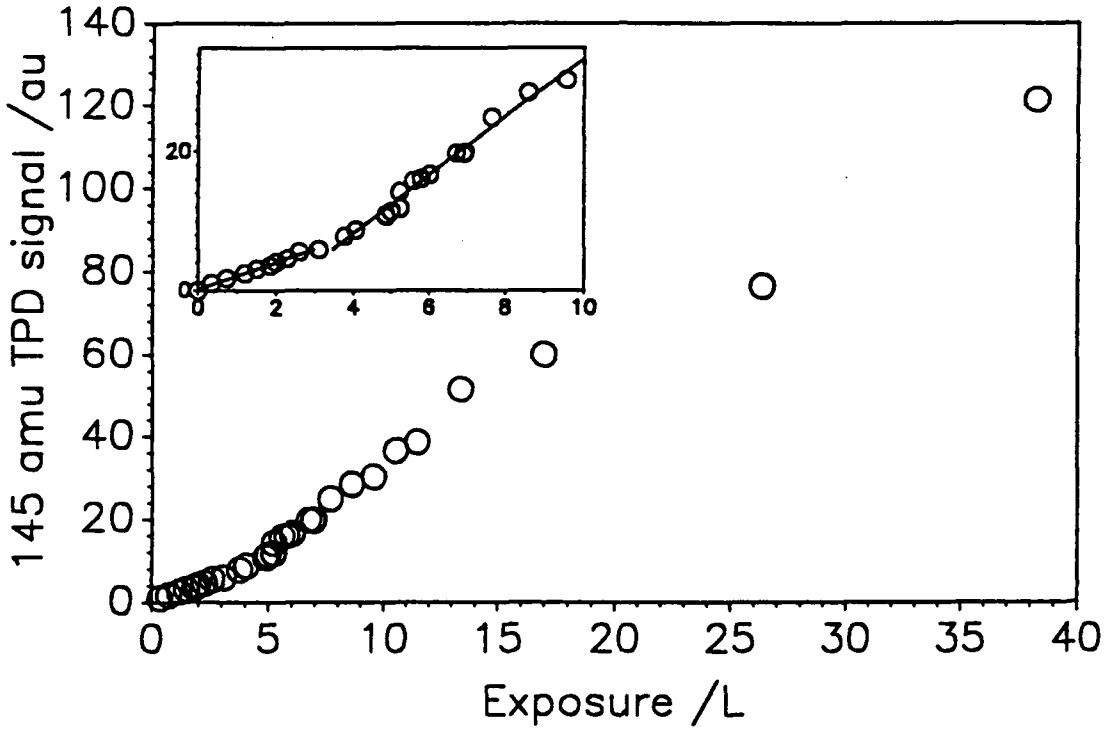

Fig 5: Plot of CD_3I exposure (measured at the chamber ion gauge) versus total intensity of the 145 amu peak measured by the UTI mass spectrometer from the TiO_2 surface during desorption experiments (directly proportional to surface coverage).

Fig 5 (Inset): The 0-10 L exposure regime on an expanded scale showing the change in uptake at approximately 3-4 L.

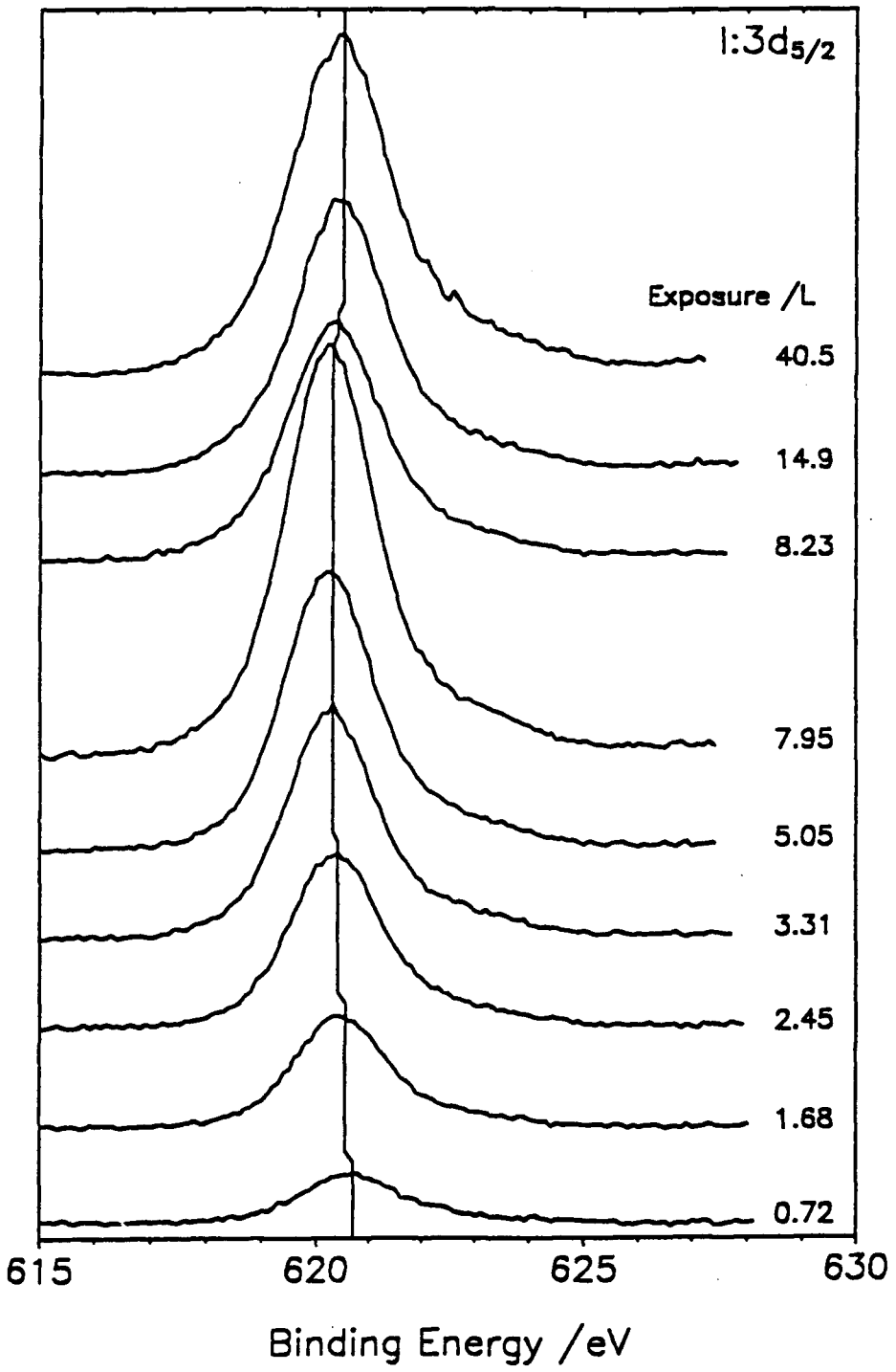

Fig 6: Change in I:$3d_{5/2}$ core level photoelectron peak with CD_3I exposure. The vertical line drawn through the peaks is a guide to illustrate the changes in the binding energy.

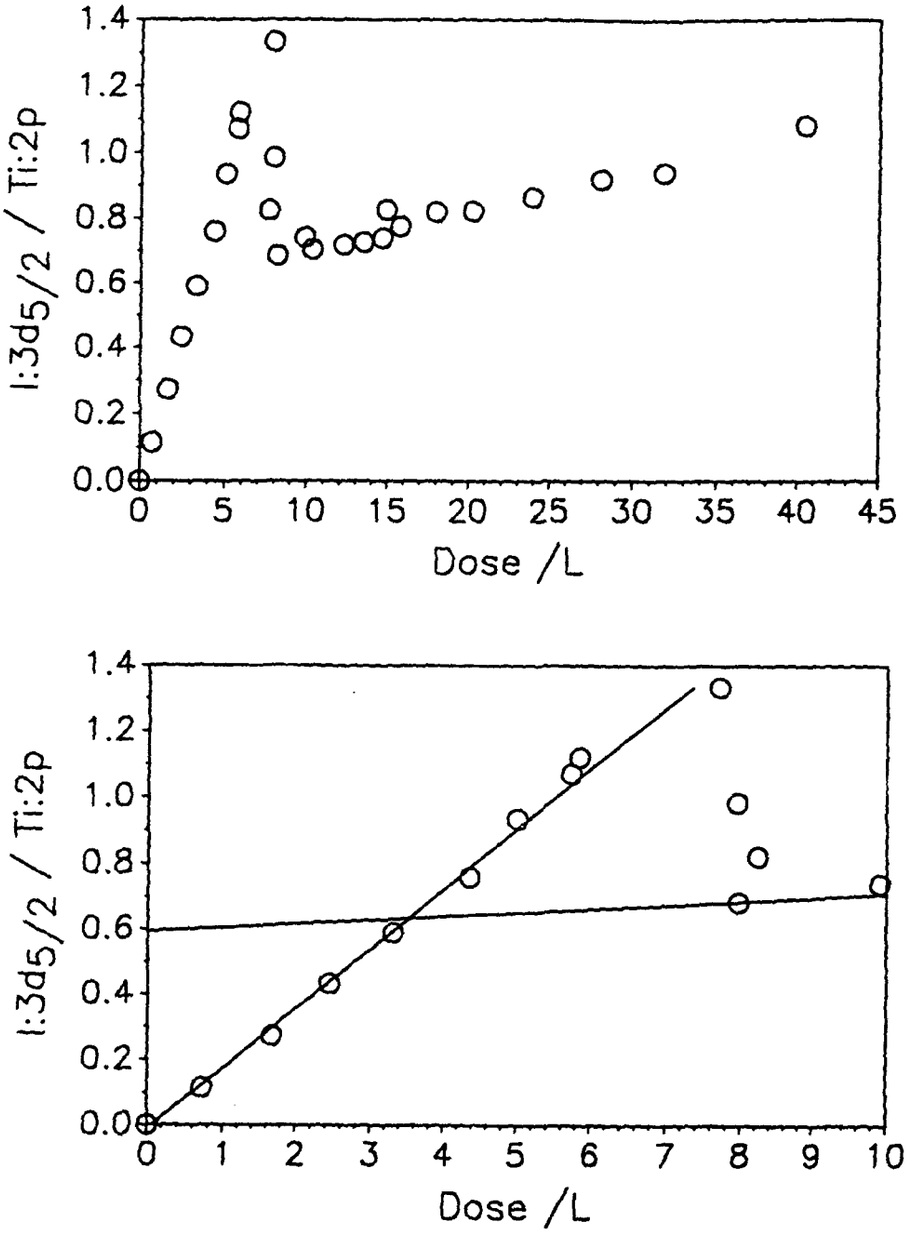

Fig 7(a)(Upper panel): I:$3d_{5/2}$/Ti:2p photoelectron peak intensity ratio with CD_3I exposure on the TiO_2(110) surface at approximately 108 K.

Fig 7(b)(Lower panel): I:$3d_{5/2}$/Ti:2p photoelectron peak intensity ratio for CD_3I exposures up to 10 L on the TiO_2(110) surface at approximately 108 K. The lines through the data represent separate linear regression fits to the 0-7.8 L data points, and the 8.0-42 L data points.

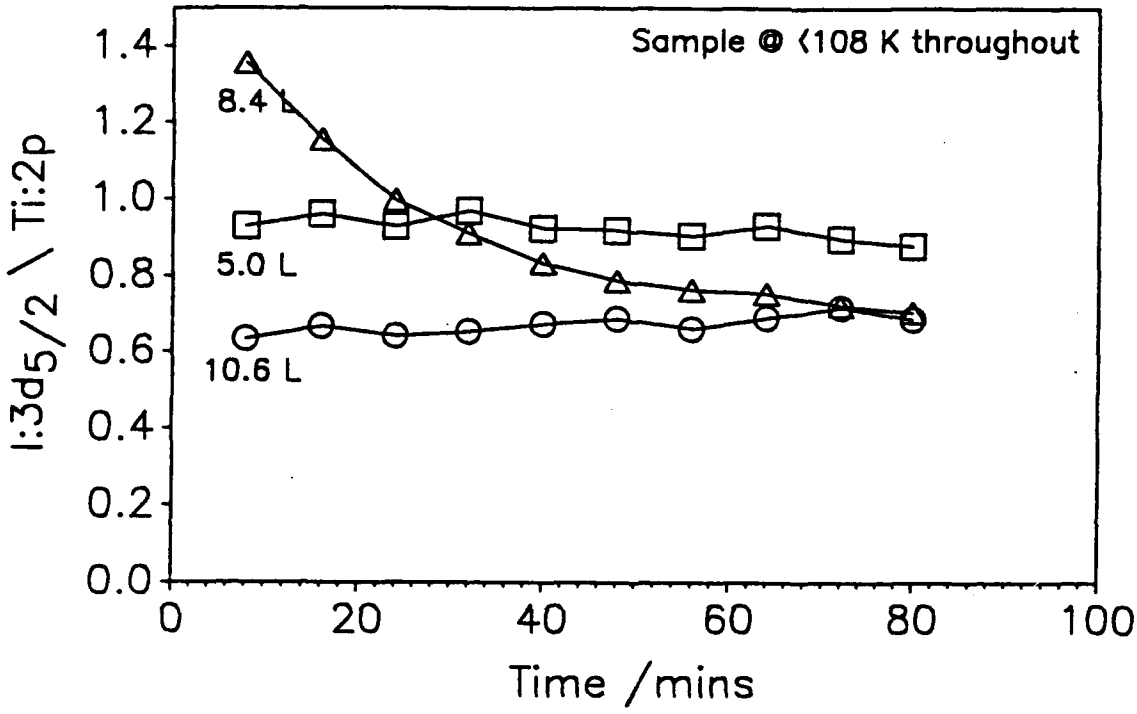

Fig 8: I:3$d_{5/2}$/Ti:2p XPS peak intensity ratios with time for 8.4, 5.0 and 10.6 L CD_3I exposures with the sample temperature fixed at 106-108 K.

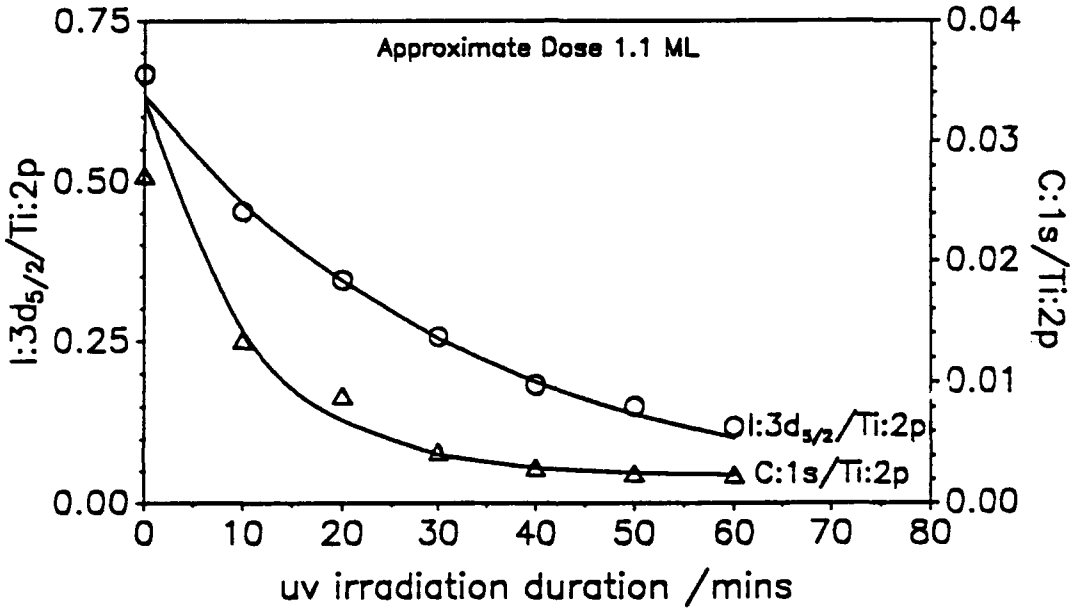

Fig 9: Decrease of both I:$3d_{5/2}$/Ti:2p and C:1s/Ti:2p XPS intensity ratios with uv irradiation from a focussed Hg lamp source fitted with 253.7 nm bandpass filter. Power density at the surface estimated at $\simeq 4$ mW cm^{-2}.

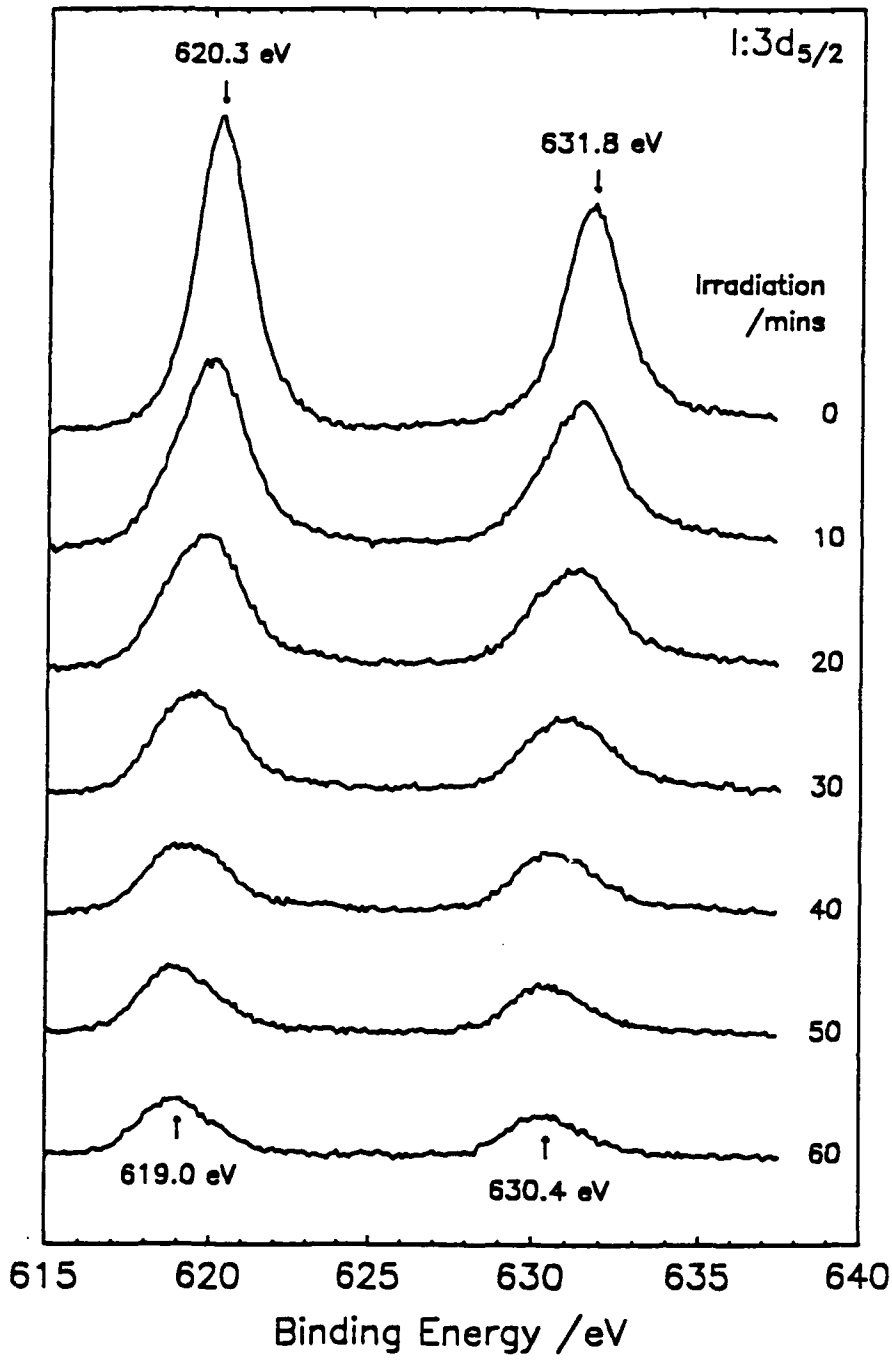

Fig 10: Changes in the I:3d core level peak envelope with uv irradiation from a focussed Hg lamp source fitted with 253.7 nm bandpass filter. CD_3I exposure of 3.3 L. (approximately 1.05 ML). TiO_2(100) surface held at < 108 K throughout.

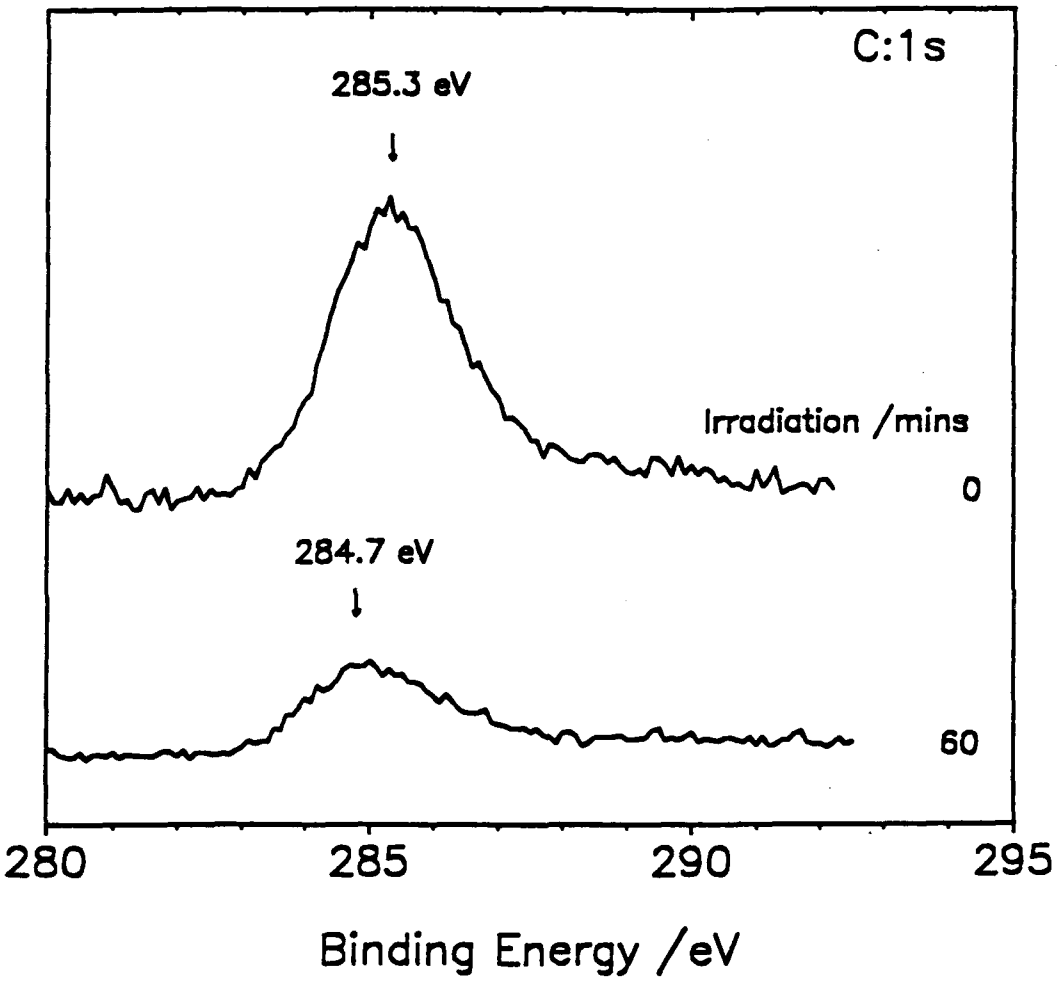

Fig 11: Changes in the C:1s core level peak envelope with uv irradiation from a focussed Hg lamp source. Experimental conditions identical to Fig 10.

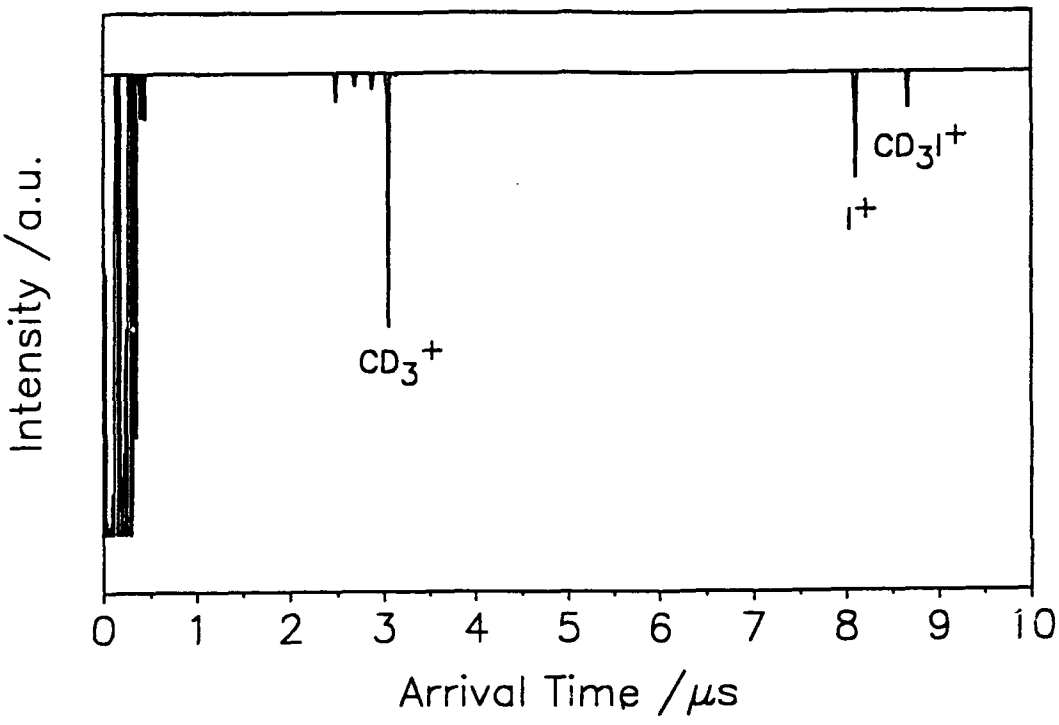

Fig 12: Typical TOF profile for gas phase CD_3I at $p=2x10^{-8}$ Torr measured with G1=1000 V, showing ions at arrival times corresponding to CD_3^+, I^+ and CD_3I^+. The structure at 0-0.5 μs is due to pick-up of scattered light by the ion detector (MCP). The probe laser was tuned to the CD_3 $3p\ ^2A_2'' \leftarrow 2p\ ^2A_2''$ (2+1) REMPI transition (resonant CD_3 ionization)

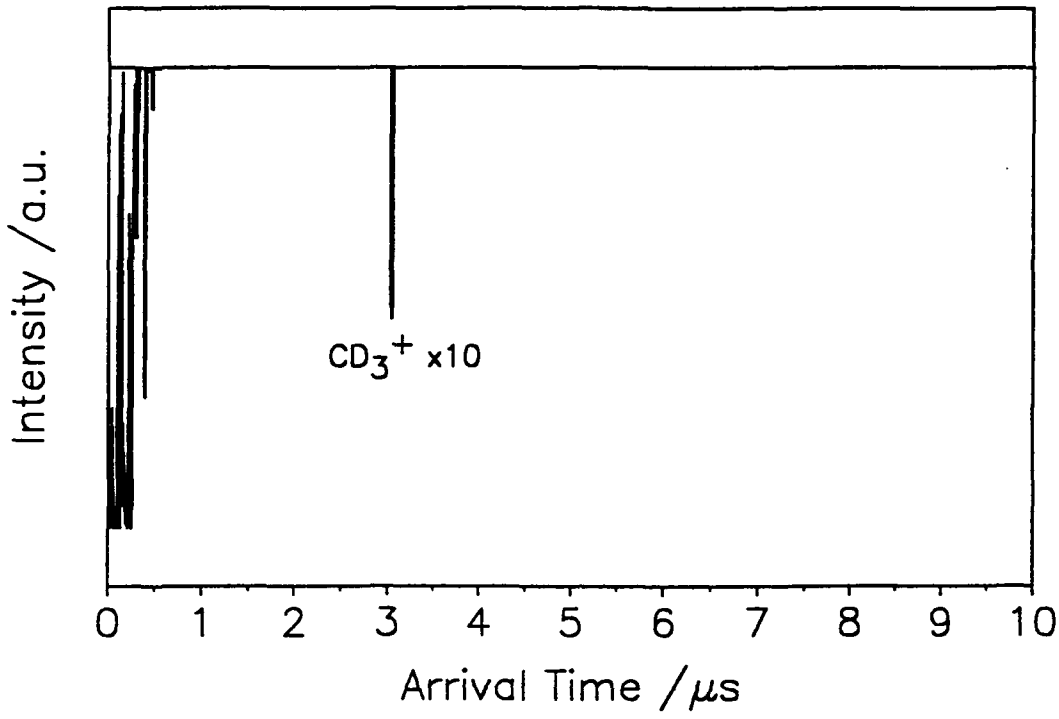

Fig 13: Typical TOF profile obtained with G1 = 1000 V, from 257 nm photodissociation of CD_3I at the 110 K $TiO_2(110)$ surface detecting photofragments in a similar manner to Fig 12. Only CD_3^+ ions are observed.

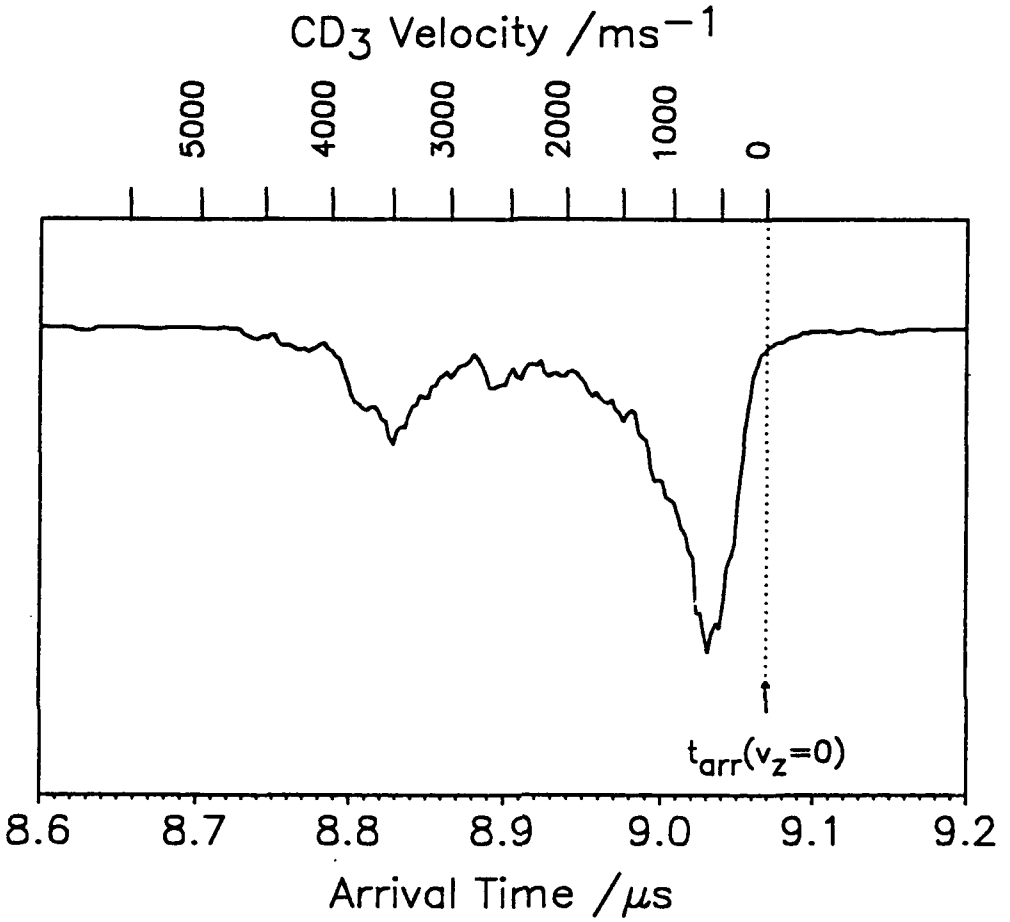

Fig 14: TOF profile for 257-nm photolysis of monolayer CD_3I on TiO_2 with G1=100 V. The $t_{arr}(v_z=0)$ line corresponds to the arrival time of CD_3 with no initial velocity along the TOF-MS flight tube axis, z. All the CD_3 photofragments from photodissociation at the surface arrive earlier than $t_{arr}(v_z=0)$ indicating they all possess some initial velocity directed along the flight tube axis.

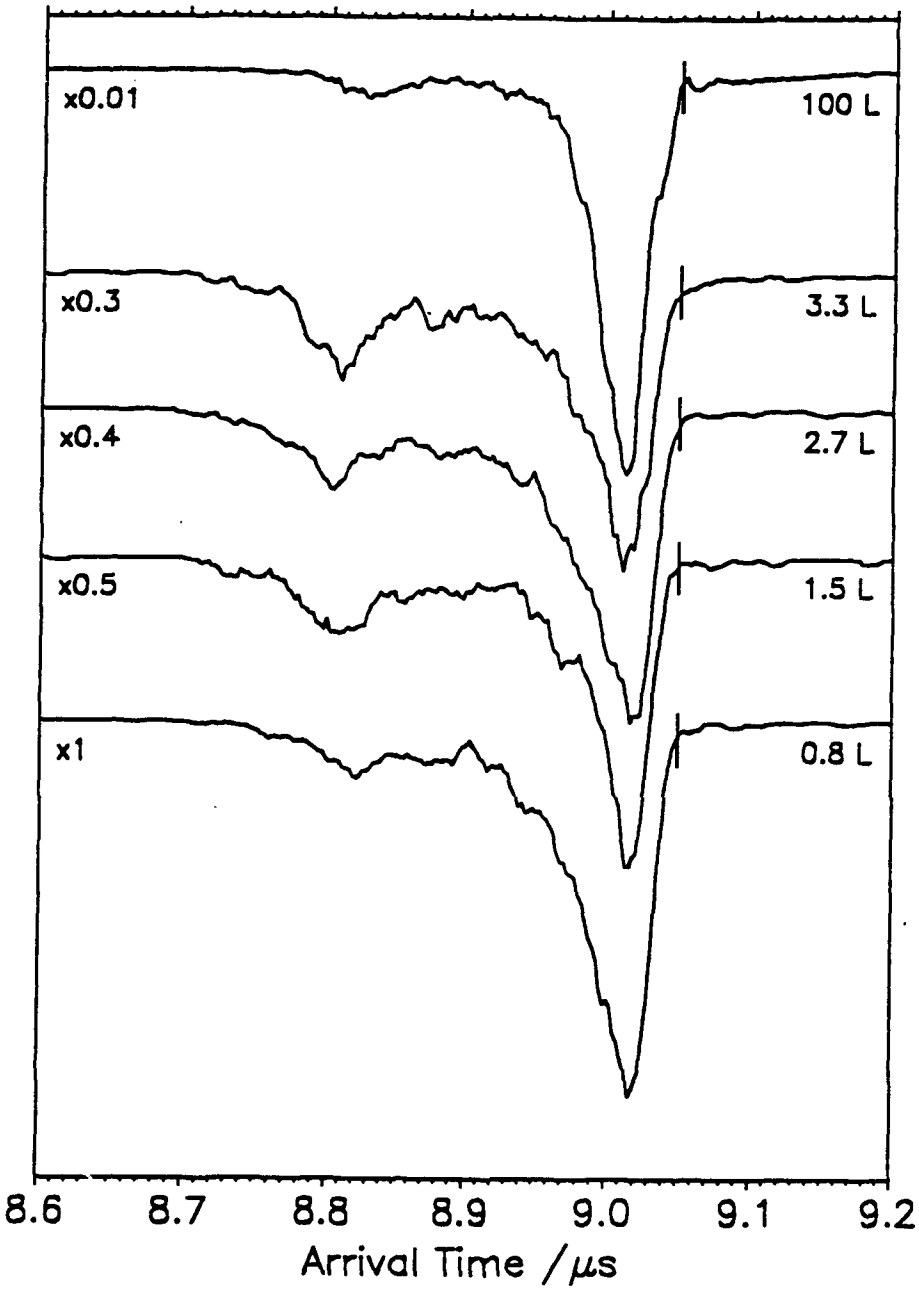

Fig 15: TOF profiles for various coverages of CD_3I on TiO_2 acquired with G1=100 V. Exposures are 0.8 L, 1.5 L, 2.7 L, 3.3 L (approximately 1 ML) and 100 L (multilayer). The short vertical lines crossing each profile at ~9.051 μs corresponds to $t_{arr}(v_z=0)$.

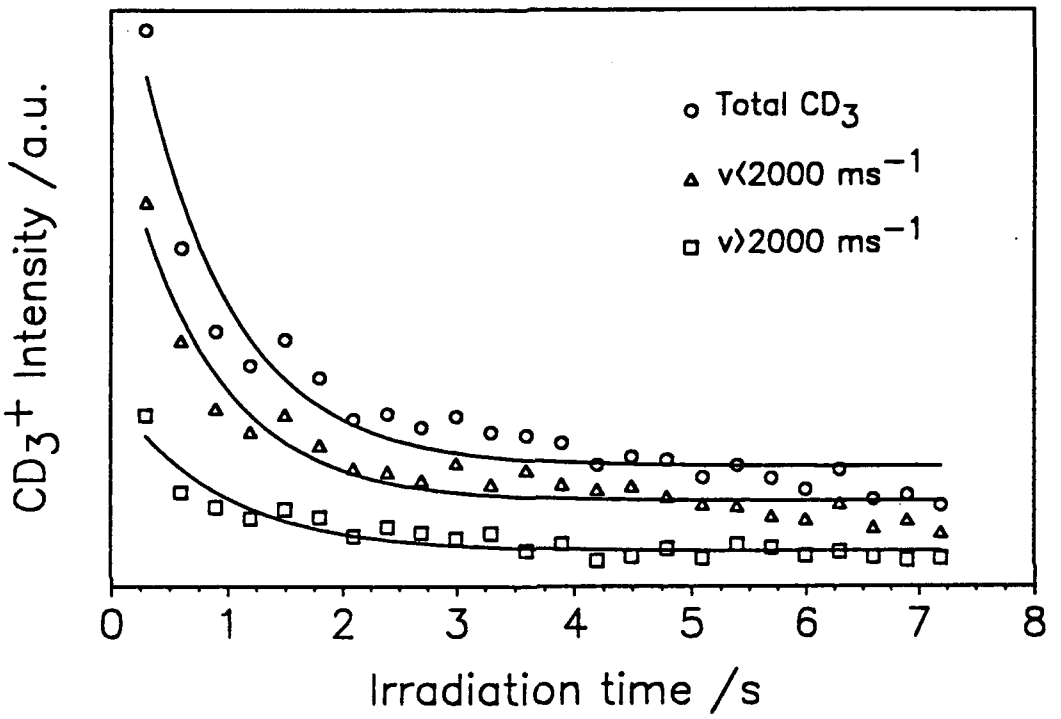

Fig 16: Total CD_3^+ signal intensity for 257 nm irradiation of approximately 1 ML CD_3I adsorbed on the 110 K TiO_2(110) surface. Data is shown for selected methyl velocities, and for the total ion signal. Each data point series has been fitted to a single exponential decay curve, therefore the "$v < 2000$ ms^{-1}" and "$v > 2000$ ms^{-1}" fitted curves may not necessarily sum to equal the "Total CD_3" fitted curve.

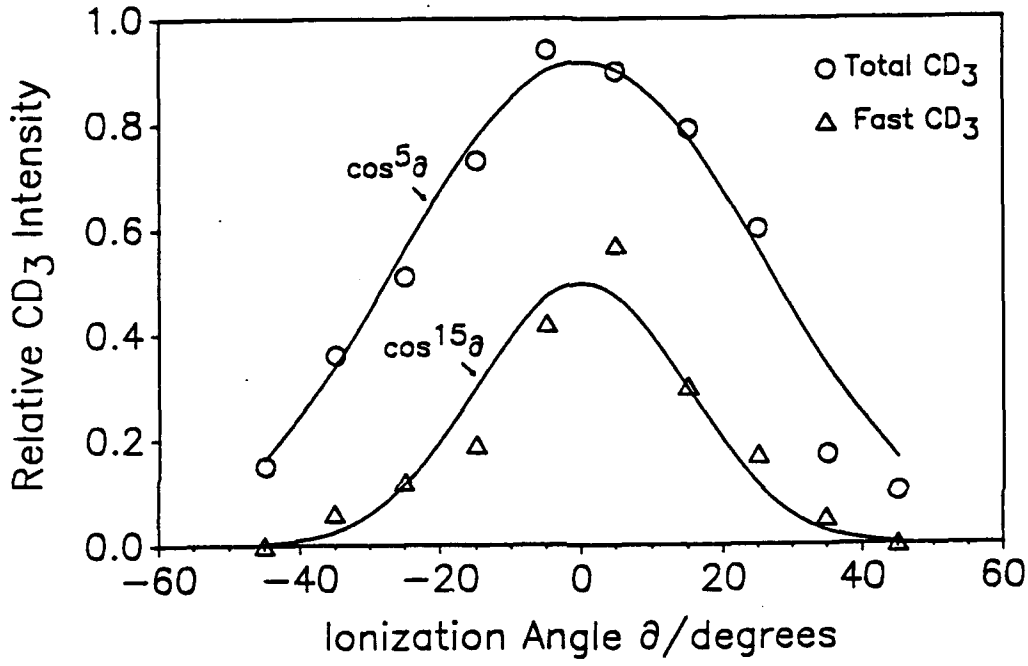

Fig 17: Angular variation of velocity selected CD_3^+ intensity obtained for multilayer CD_3I coverage. Determined with G1 = 1000 V and rotation of the probe beam in an arc above the surface photolysis point. "Fast" $CD_3 \equiv CD_3(2000 < v < 20000\ ms^{-1})$ and "Total" $CD_3 \equiv (200 < v < 20000\ ms^{-1})$. The curves drawn through the data are not intended to be "fits" to the data points.

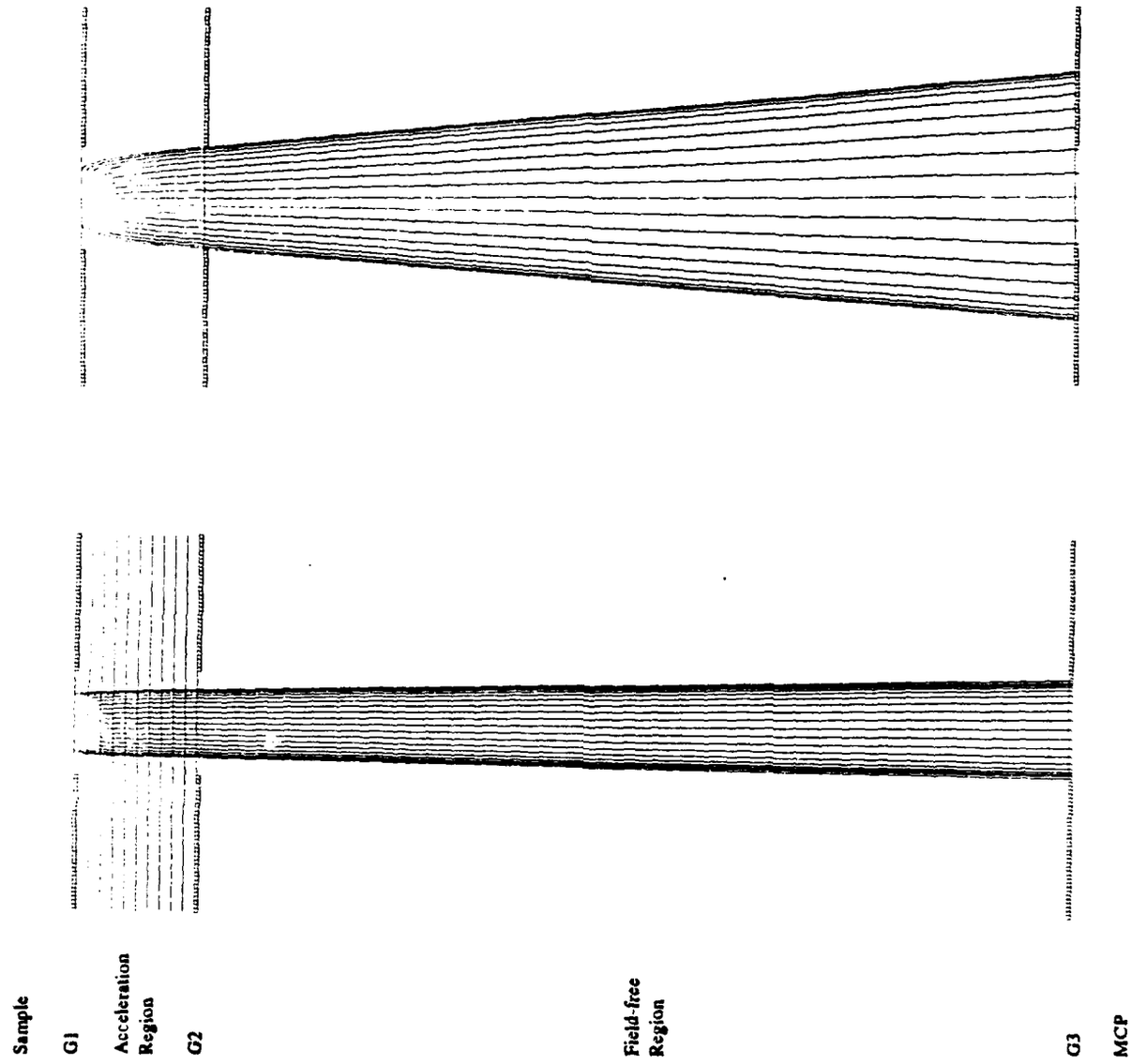

Fig 18: Simulations[20] of CD_3 ion trajectories for various photoejection angles, in 10° steps, away from the surface normal. Obtained for various repeller (G1) voltages with initial CD_3 velocity of 3500 ms^{-1}. Cross-section along the TOF-MS axis, z.

(Upper panel): Simulated trajectory of CD_3 fragments, ionized at 3mm from the surface located immediately to the left of G1 with G1 = 100 V.

(Lower panel): As upper panel but G1 = 1000 V. Lines of equivalent potential are shown at 100 V intervals between G1 and G2.

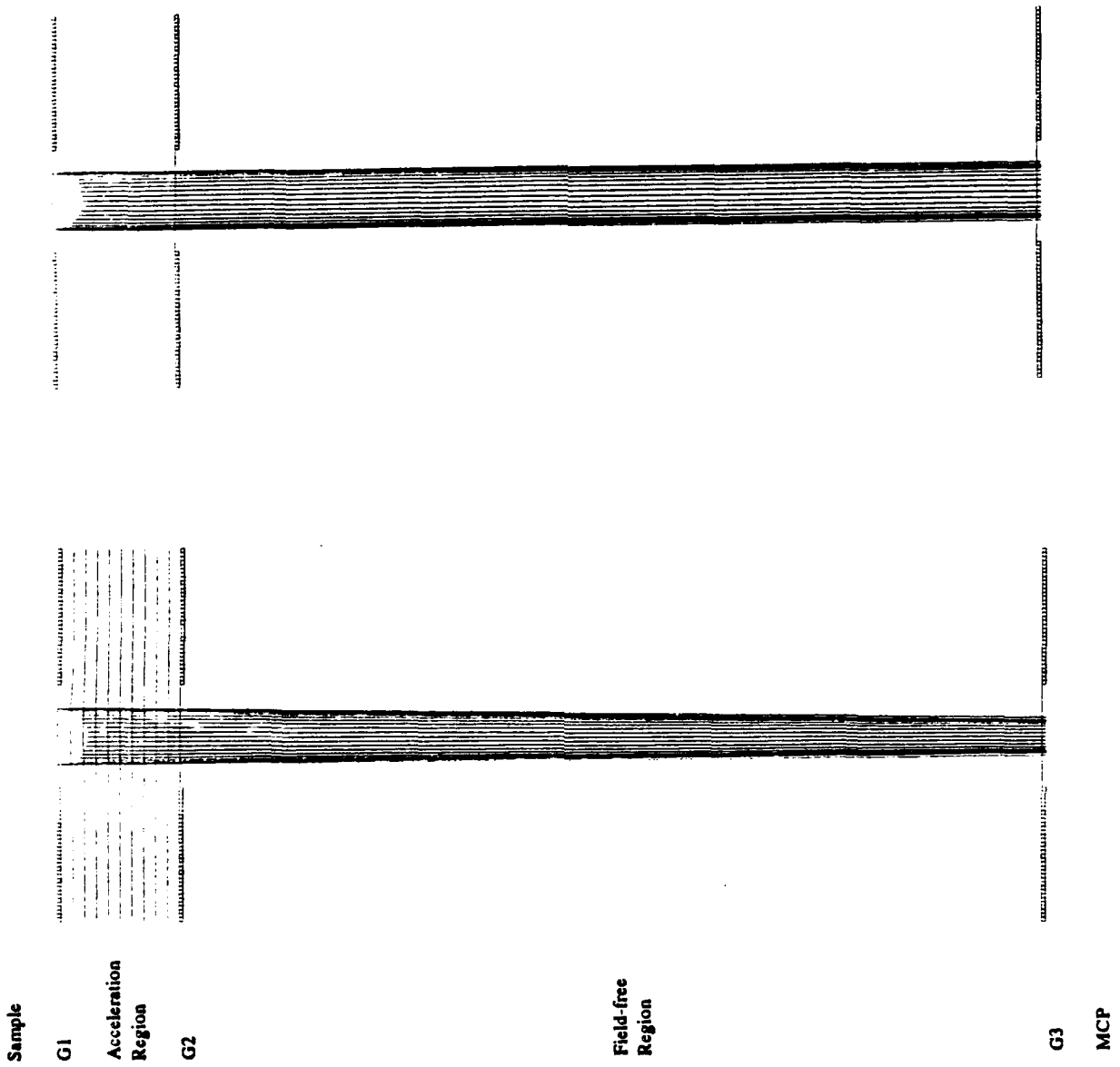

Fig 19: Simulations[20] of CD_3 ion trajectories for various photoejection angles, in 10° steps, away from the surface normal. Obtained for various repeller (G1) voltages with initial CD_3 velocity of 500 ms^{-1}. Cross-section along the TOF-MS axis, z.

(Upper panel): Simulated trajectory of CD_3 fragments, ionized at 3mm from the surface located immediately to the left of G1 with G1 = 100 V.

(Lower panel): As upper panel but G1 = 1000 V. Lines of equivalent potential are shown at 100 V intervals between G1 and G2.

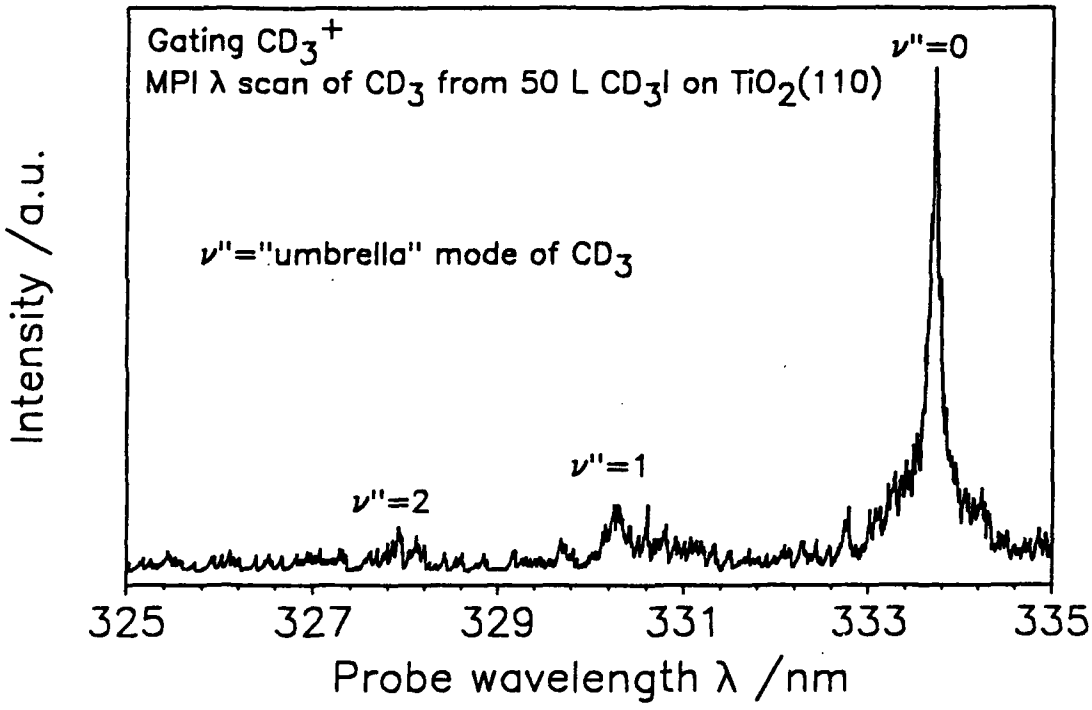

Fig 20: Overall vibrational population distribution of CD_3 photofragments produced by 257 nm laser irradiation of a CD_3I multilayer covered $TiO_2(110)$ surface obtained by scanning the probe laser wavelength through the (2+1) REMPI transitions of each of the vibrational states.

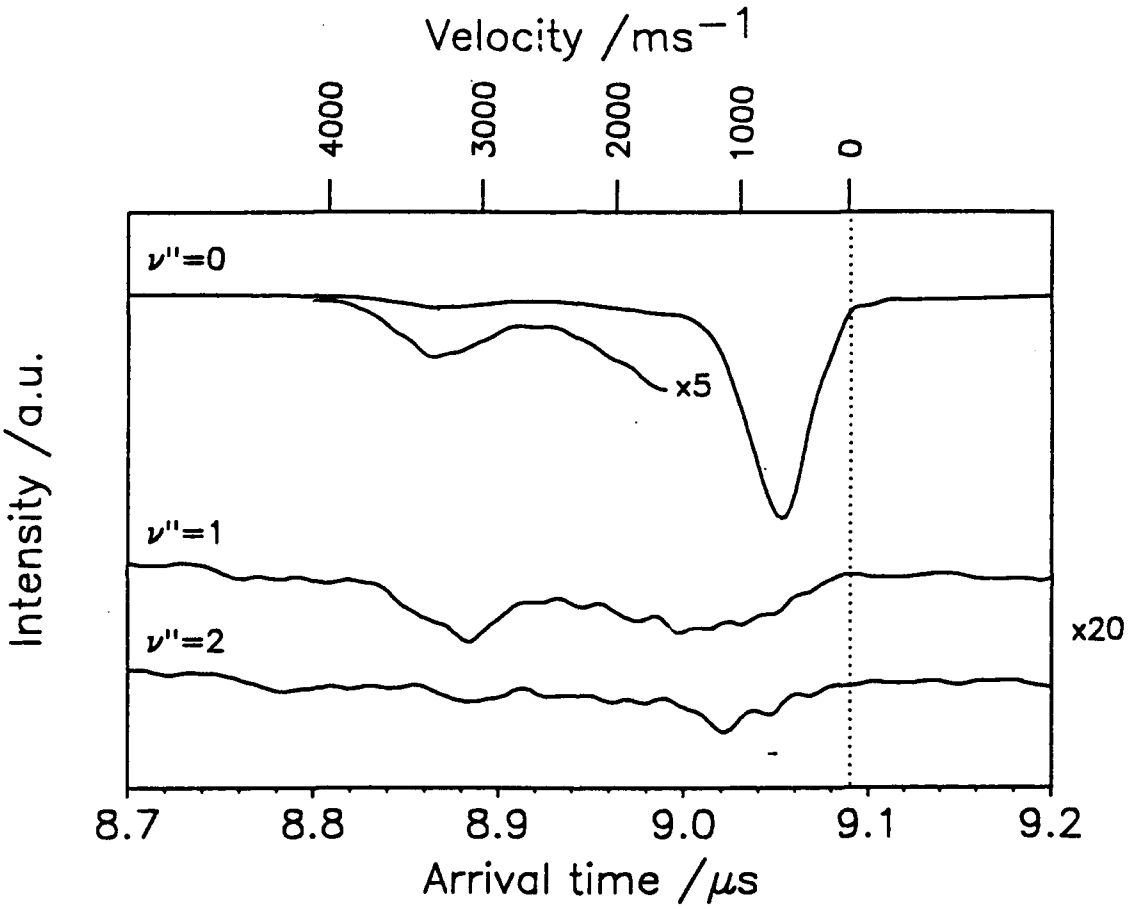

Fig 21: TOF profiles for multilayer coverage of CD_3I measured with G1=100 V. The profiles were obtained by fixing the probe laser wavelength at the center of the CD_3 $v''=0$, $v''=1$ and $v''=2$ bands.

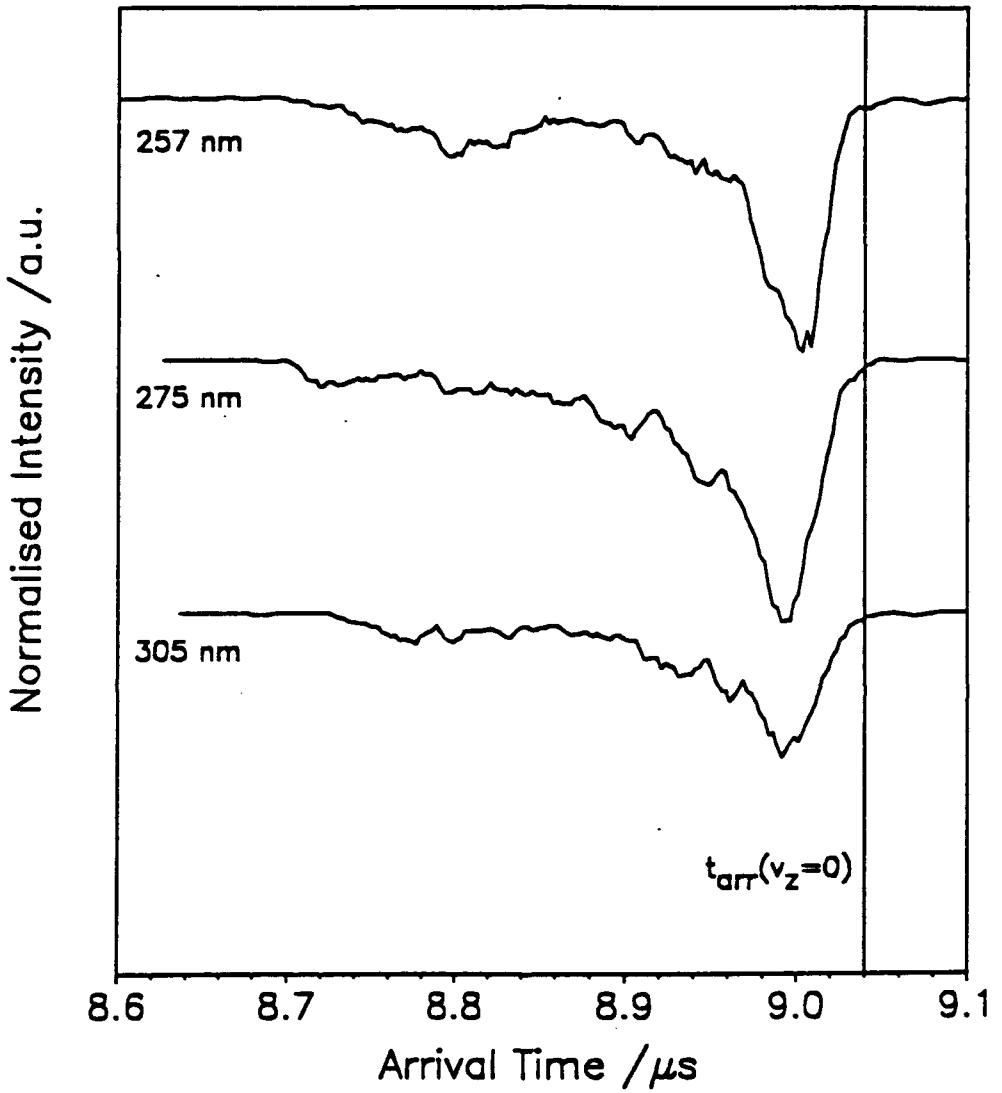

Fig 22: TOF profiles for 257, 275, 305 nm photodissociation of monolayer CD_3I on $TiO_2(110)$. Measured with G1 = 100 V with the probe laser fixed at the center of the CD_3 ($v''=0$) band.